Diamond formation beneath the Coromandel area, southwestern São Francisco Craton – The role of re-fertilization and subduction

Luísa D.V. Carvalho [a b] *, Thomas Stachel [b], D. Graham Pearson [b], Reinhardt A. Fuck [c], Tiago Jalowitzki [c], Suzette Timmerman [b], Matthew Steele-Maclnnis [b], Guilherme O. Gonçalves [c], Rogério Silvestre Pereira [c], Ricardo Scholz [a].

[a] Universidade Federal de Ouro Preto (UFOP), Escola de Minas, Departamento de Geologia, Campus Morro do Cruzeiro, 35400-000, Ouro Preto, MG, Brazil

[b] University of Alberta, Department of Earth and Atmospheric Sciences, 1-26 ESB, Edmonton, AB, T6G 2E3, Canada

[c] Universidade de Brasília (UnB), Instituto de Geociências, Campus Universitário Darcy Ribeiro, 70910-900, Brasília, DF, Brazil

*Corresponding author

Luísa D.V. Carvalho

e-mail: luisa.carvalho@ualberta.ca

Abstract

The lithospheric mantle underpinning the Alto Paranaíba Igneous Province, southwestern São Francisco Craton, was investigated through a study of 82 diamonds and their mineral inclusions from the Coromandel (Douradinho River), Verde River (northern Coromandel), Abaeté, Frutal, and Romaria deposits. Mineral inclusion abundances show that lherzolite is the main diamond source-rock, followed by eclogite, harzburgite and minor websterite. The limited chemical depletion recorded in lherzolitic inclusions suggests a post-Archean origin or modification of the lithospheric mantle beneath this part of the São Francisco craton. Sinusoidal rare earth element patterns for lherzolitic garnet inclusions indicate variable but overall low degrees of metasomatism by fluids or silico-carbonatitic (proto-kimberlitic) melts. These results contrast with previous studies on mineral inclusions in diamonds (Canastra range, southern Coromandel; Rio da Prata system, northeastern Coromandel; our new data on the Frutal area, southwestern Coromandel),

where a dominance of harzburgitic inclusions documents a more depleted, likely Archean, cratonic root. Bulk rock compositions reconstructed from eclogitic and websteritic inclusions establish a clear link between subduction processes and diamond formation in the Coromandel region. Calculated bulk rare earth element patterns match typical sections of upper oceanic crust, where plagioclase accumulation is uncommon. Pyroxene inclusion-based geothermobarometry indicates that lherzolitic and websteritic diamonds formed and last resided along a ~39 mW/m² model geotherm. Projection of eclogitic garnet-clinopyroxene pairs onto this 39 mW/m² geotherm places their origin near the base of the lithosphere (> 180 km depth). Low nitrogen contents and high aggregation states (up to 100 %B) indicate that eclogitic, websteritic, and part of the lherzolitic diamond populations experienced extended (2.0 Byr) mantle residence at high temperatures (> 1200 °C). The similarity in mantle residence temperatures and the shared presence of minor negative Eu anomalies for eclogitic and websteritic diamonds and their inclusions may be indicative of a common origin, following emplacement of subducted oceanic crust beneath the São Francisco Craton margin likely during a Paleoproterozoic orogeny (2.2-1.9 Ga). Based on our results, future exploration efforts in the Alto Paranaíba region should shift their focus from harzburgitic to lherzolitic and eclogitic indicator minerals to find new diamond deposits and kimberlites in this area.

Keywords: Inclusions in diamonds. São Francisco Craton. Alto Paranaíba Igneous Province. Geothermobarometry. Nitrogen aggregation. Eclogite.

1. Introduction

Diamond formation in the mantle is considered to be a metasomatic process. The agents of metasomatism, melts or supercritical fluids, react with the mantle rocks and diamond crystallizes either isochemically, as a consequence of cooling and oversaturation in carbon, or in the course of wall-rock buffered redox reactions (Stachel and Luth 2015). Unlike other mantle minerals, diamond is chemically inert, isolating its mineral inclusions from subsequent metasomatic modification. The study of inclusions in diamond allows to characterize the rocks that form the substrates for diamond precipitation, revealing that among lithospheric diamonds worldwide, 65% are derived from peridotitic sources, 33% are eclogitic and 2% websteritic (Stachel and Harris 2008). Sublithospheric diamonds, from the asthenosphere, transition zone and lower mantle, are rare and account for only about 1-2 % of the worldwide diamond production. Mineral inclusions in diamonds, therefore, primarily provide pristine information on both the nature and origin of the subcontinental lithospheric mantle and the origin of its diamond endowment.

The presence of alluvial diamonds and their close spatial association to mantle-derived igneous rocks of the Alto Paranaíba Igneous Province (APIP) bring into focus the gaps in our understanding of the origin and evolution of the lithospheric mantle beneath the southwestern margin of the São Francisco Craton. Diamonds studied here are all derived from alluvial deposits and their primary volcanic sources are still unknown. Pereira et al. (2017, and references therein) recognize evidence of young, proximal, and primary sources for diamonds from the same context. From our visual observation alone, diamond populations from each of the alluvial deposits have a unique set of physical characteristics and these first order distinctions are further confirmed by the analytical results presented in this study (e.g., through distinct nitrogen characteristics and inclusion chemistries). We, therefore, regard the studied diamonds as being relatively proximal (within a few tens of km at most) to their primary sources, rather than reflecting craton-scale mixing of diamonds from multiple sources.

In the southwestern part of the São Francisco Craton, the occurrence of valuable alluvial diamonds and kimberlites related to the APIP stimulated decades of exploration for the primary sources of diamonds, from the late 1960's to the 2000's. Diamonds in the APIP are especially sought after due to the common occurrence of sizable stones (>100 ct). Such large stones are particularly abundant in the context of three rivers that run parallel in SE-NW orientation, immediately south of the town of Coromandel, named Douradinho, Santo Inácio and Santo Antônio do Bonito (Pereira and Fuck 2005). In the Santo Antônio do Bonito River, the largest gem diamond ever found in Brazil was recovered in 1938, weighting 726.6 ct. Throughout the years, the Coromandel and Abaeté areas have also produced a considerable amount of high-value pink stones.

Diamond exploration in the Alto Paranaíba region, largely based on indicator minerals, culminated in the discovery of the hundreds of intrusive bodies known to date. Despite these discoveries, the evaluation techniques applied at the time classified most of the kimberlites as non-economic, and exploration companies left the area at the beginning of the 2000's. In the APIP, only a few kimberlites are known to be diamondiferous and no link to the valuable alluvial diamond deposits could be established so far. Although a large number of intrusions are already known in the APIP, as the erosion of the Cretaceous Mata da Corda Group progresses, new Cretaceous intrusions are being revealed, such as the recently discovered Osvaldo França 1 kimberlite (Carvalho et al. 2022).

To map the nature of the lithospheric mantle beneath the APIP, we present the first study on diamonds and their mineral inclusions from this area. We analyzed the nitrogen systematics of the host diamond along with the major and trace element composition of their mineral inclusions, focusing on diamonds from the Douradinho River, Verde River, Abaeté, Romaria, and Frutal deposits. Geothermobarometry of the inclusions and nitrogen thermometry of the diamonds aids in understanding

the formation conditions of the diamonds and their lithospheric residence. The composition of the mineral inclusions is used to determine the nature of the diamond substrate. The paragenetic abundances in the studied diamonds provides new implications for diamond exploration.

2. Overview of the São Francisco Craton basement and the Alto Paranaíba Igneous Province

The oldest components so far identified in the São Francisco Craton date back to 4.1 Ga, and events recorded up to 2.5 Ga indicate stabilization of the cratonic nuclei predominantly in the Neoarchean (Teixeira et al. 2017). Exposed in the southernmost and northeastern portions of the craton, Archean rocks are in direct contact with Paleoproterozoic orogenic belts that register the collision between the São Francisco and Congo paleocontinents at ~2.1-2.0 Ga, with indications of subduction-related events starting at 2.47 Ga (Alkmim and Teixeira 2017; Barbosa and Barbosa 2017). Following the development of sedimentary basins along its passive margins and in rift zones that infringed onto the cratonic nucleus, the Brasiliano Orogeny in the Neoproterozoic shaped the current outline of the São Francisco Craton (Heilbron et al. 2017). Delineating its southwestern limits, the east-verging thrust sheets of the Southern Brasília belt formed as a result of the convergence of the Amazonian, São Francisco-Congo and Paranapanema blocks, where subduction-related regional metamorphism is dated between 650 and 630 Ma (Pimentel 2016).

Cretaceous alkaline/ultramafic magmatism, structurally controlled by the Azimuth 125 lineament (Bardet 1977), intruded the metasedimentary rocks of the Brasília belt in western Minas Gerais and eastern Goiás states, giving rise to the APIP (**Fig. 1**). At that time, the Brasília belt acted as a topographic high, separating the distribution of sediments between the Paraná basin to the west, and São Francisco basin to the east. The volcanoclastic deposits of the APIP are mainly of kamafugitic affinity and comprise the Mata da Corda Group, the upper Cretaceous section of the São Francisco basin, and time-equivalent occurrences in the Paraná basin (**Fig. 1**). Although intruding metasedimentary rocks of the Neoproterozoic Brasília mobile belt, several studies have shown that all APIP rock types were likely sourced from the subcontinental lithospheric mantle (e.g., Carlson et al. 1996). The lithospheric mantle beneath the Alto Paranaíba area, at a depth of 150 km, is characterized by low seismic velocities (Carvalho et al. 2022), contrasting high velocities in the cratonic nucleus (Rocha et al. 2019). Tomographic (Rocha et al. 2019) and gravimetric (Pereira and Fuck 2005) data indicate that the cratonic lithosphere of the São Francisco Craton extends underneath the Brasília Belt.

3. Samples and Methods

Our study is based on 82 diamonds recovered from artisanal mines in the southwestern part of the São Francisco Craton. Most diamonds are from placer deposits of the Abaeté (n=6), Douradinho River (n=25) and Verde River (n=27), and from a Cretaceous conglomerate at Romaria (n=11). In addition, this study examined diamonds from placer deposits at Frutal (n=13), in westernmost part of study area. The Frutal placer deposits may have received some contribution - via sediment transport - from the APIP areas, but such a contribution is currently debated and unconstrained (**Fig. 1**). In all figures, a specific color is used for each sample locality: orange = Abaeté; blue = Douradinho River; grey = Frutal; yellow = Romaria; green = Verde River. The first two letters of all sample numbers indicate the sample location: AB = Abaeté, DR = Douradinho River, FT = Frutal, RM = Romaria, VR = Verde River.

Sample preparation and analyses were performed using facilities at the University of Alberta, Canada. Ranging in mass from 0.08 to 2.2 ct, the diamonds were broken using a steel-crusher for the recovery of mineral inclusions and analysis of diamond fragments.

Diamond fragments were analyzed for their nitrogen concentrations and aggregation states using a micro-Fourier transform infrared spectrometer (µ-FTIR), Thermo Fisher Nexus 470, attached to a Continuum IR microscope. The detector was cooled with liquid nitrogen. Using a squared aperture size of 100 µm, spectra were taken in transmission mode over the range of 4000 to 650 cm^{-1} by averaging 200 scans with a resolution of 4 cm^{-1}. Spectral deconvolution and nitrogen quantification were accomplished following the procedure described in Stachel et al. (2018a).

Mineral inclusions were recovered from 21 diamonds via cracking. The inclusions were mounted individually in epoxy resin in 6 mm brass pips and polished for microprobe analysis. Major and minor element concentrations were measured using a JEOL JXA-8900R EPMA with an accelerating voltage of 20 kV and a beam current of 30 nA. For a sulfide inclusion, an accelerating voltage of 15 kV was used. Peak count times were 15–20 s and background time was half the peak time, resulting in oxide detection limits of typically ≤ 0.02 wt%. Al, Ca and Cr trace concentrations in olivine were measured using a CAMECA SX100 Electron Probe Microanalyzer (EPMA) with an accelerating voltage of 20 kV and a beam current of 300 nA. The detailed protocols of olivine trace element analysis using EPMA are given in Bussweiler et al. (2019). Our analyses of reference material SC-GB agree within uncertainty with the values stated in that study. For all microprobe analyses, three spots on average were measured per sample and, after assessing compositional homogeneity, averaged.

Trace element concentrations of garnet and clinopyroxene inclusions were analyzed using a Resonetics M-50-LR 193 nm ArF excimer laser ablation system with a Laurin-Technic S-155 two-volume ablation cell coupled to a Thermo Scientific Element IIXR inductively coupled plasma mass spectrometer

(ICP-MS). Depending on the inclusion size, samples and standards were ablated with a spot size of 15 to 90 µm at a frequency of 10 Hz and a laser fluence of ~3.5 J/cm^2. Trace elements were measured on the following masses: ^{45}Sc, ^{49}Ti, ^{85}Rb, ^{88}Sr, ^{89}Y, ^{90}Zr, ^{93}Nb, ^{137}Ba, ^{139}La, ^{140}Ce, ^{141}Pr, ^{146}Nd, ^{147}Sm, ^{153}Eu, ^{157}Gd, ^{159}Tb, ^{163}Dy, ^{165}Ho, ^{166}Er, ^{169}Tm, ^{172}Yb, ^{175}Lu, ^{178}Hf, ^{180}Hf and ^{181}Ta. Each spot analysis consisted of 40 s of background acquisition and 60 s of sample ablation, followed by a wash time of 40 s. For spot sizes from 23 to 90 µm, NIST SRM 612 glass was used as the primary standard and NIST614 was used as a quality control. For spot sizes of 15 µm, NIST SRM 610 was used as the primary standard and NIST612 to assess the accuracy of the concentrations. ^{43}Ca contents, previously measured by EPMA, were used as internal standard. The agreement of values measured for secondary standards was better than 10% for all spot sizes employed.

For some mineral phases, their chemical structure was confirmed via Raman spectroscopy. Raman spectra were collected using a Horiba Scientific's LabRAM HR Evolution mounted with an Olympus optical fiber microscope. Using a monochromatic laser with a 532 nm frequency, Raman spectra were collected using 3 accumulations, acquisition time of 30 seconds, and 50% laser intensity.

4. Results

4.1. Diamonds characteristics

All diamonds were examined for their color, morphology, surface features, and nitrogen characteristics. Colors range from colorless to brown, with additional yellowish/yellow and rare pink and greenish samples. Most diamonds are intensely resorbed and dodecahedral shapes predominate. Widespread surface features are hillocks, plastic deformation lines and minor frosting. In addition, edge abrasion related to alluvial transport is widespread. The occurrence of irradiation-induced green and brown spots on diamond surfaces is restricted to the Verde River and Frutal populations.

Figures 2a and **b** show the distribution of color and morphology among the five diamond populations studied. Brown diamonds principally occur in the Douradinho River, Verde River and Abaeté populations, while Frutal and Romaria diamonds are typically colorless. Considering diamond morphology, Douradinho River has a unique population of flat dodecahedrons, and two hemimorphic diamonds occur. Less resorbed octahedral and transitional dodecahedral-octahedral morphologies are most prominent in Romaria diamonds.

Nitrogen contents range from below detection (<5 at.ppm) to ~2300 at.ppm, with nitrogen abundances >1000 at.ppm being restricted to diamonds from Frutal and Romaria (**Fig. 2c**). For ~10% of

the diamonds, significant intra-crystal variations in nitrogen content (>300 at.ppm) were detected; in these cases, rims are generally lower in nitrogen content and aggregation state. The full range in aggregation (0-100 %B with $\%B=100N_B/(N_A+N_B)$) from pairs of nitrogen (A-centres) to four nitrogen around a vacancy (B-centres) was observed. Douradinho River diamonds are distinct by an unusual dominance (56%) of high aggregation states (>89 %B; **Fig. 2d**) and a high proportion (~30%) of diamonds with [N] <12 ppm (mainly as Type IaAB). At Frutal and Romaria, low to intermediate (0-67 %B) aggregation states dominate. Despite high nitrogen aggregation states of Douradinho River diamonds, the planar defects (platelets) invariably associated with the formation of B centers (Woods 1986) are not common. Plastic deformation, which is widespread among samples from Douradinho River, or thermal pulses are regarded as causes for platelet degradation (Woods 1986; Evans et al. 1995). Approximately 80% of the diamonds show hydrogen-related impurities (absorbance at 3107 cm^{-1}). Overall, Frutal diamonds have the strongest hydrogen-related absorbance, with no relationship to total nitrogen contents. A positive correlation between N and H contents is, however, recognized for diamonds with eclogitic inclusions. The single websteritic diamond from Douradinho River is also notably hydrogen-rich.

4.2. Mineral inclusions

Mineral inclusions from 21 diamonds were analyzed for major and trace element compositions. Four locations are represented among these diamonds, as indicated in **Table 1.** No inclusions were recovered from Romaria diamonds. Inclusions range in size from ~30 to 500 μm (**Fig. 3**), and mainly display cubo-octahedral morphologies imposed by their host diamonds. Chemically identified minerals, in order of decreasing abundance, are olivine, omphacite, enstatite, Cr-diopside, pyrope-almandine, Cr-pyrope, Mg-chromite, coesite and sulfide. Based on inclusion chemistry (**Supplementary Data 1**), diamonds are assigned to the peridotitic (n=14), eclogitic (n=6) and websteritic (n=1) suites (**Table 1**).

4.2.1. Major element chemistry of peridotitic/websteritic inclusions

Olivine was recognized in 10 diamonds, mainly as multiple colorless inclusions of a single phase or together with enstatite, Cr-diopside and garnet. In one case, olivine forms a touching, graphite-coated pair with a Cr-diopside (**Fig. 3a and b; Supplementary Fig. 1a**). Graphite-coating of olivine is widespread among Douradinho River diamonds (**Fig. 3a and c**). Olivine Mg# (molar 100Mg/(Mg+Fe)) varies from 91.2 to 94.4. For three diamonds of lherzolitic paragenesis (based on co-occuring Cr-diopside inclusions), olivine Mg# ranges from 91.5 to 92.0. Calcium contents reveal two distinct groups; a high-Ca group (CaO > 340 ppm), in which samples display positive correlations of Ca with Cr and Al, and a low-Ca group (CaO < 215 ppm), in which such correlations are absent (**Fig. 4a**). Olivines from the low-Ca group all have Mg# >93 and are likely of harzburgitic paragenesis (Stachel and Harris 2008). Olivines in the high-Ca group

have Mg# <92.5 and are likely lherzolitic, especially as this group includes all samples of known lherzolitic paragenesis. Douradinho River olivines display the highest Cr_2O_3 contents in both the low- and high-Ca groups.

Colourless to faint green **enstatite** occurs in five diamonds, both as single crystals and touching with clinopyroxene (**Fig. 3d and *5*a**). Mg# ranges from 92.8 to 94.0, with the exception of one enstatite (Mg# 89.4) touching with a clinopyroxene in a Douradinho River diamond (**Fig. 5b**). The low Mg-number of the latter is comparable to enstatite of the transitional websteritic-lherzolitic association in diamonds from Voorspoed, South Africa (Viljoen et al. 2018). Compared to Voorspoed websteritic and transitional websteritic-lherzolitic enstatites, the Douradinho River enstatite, however, has higher CaO (**Fig. 4b**), TiO_2, and Na_2O contents (1.25, 0.12 and 0.23 wt%, respectively). Based on its low Mg# and Cr and high Na-Ti-Mn contents, this enstatite is likely of websteritic (pyroxenitic) paragenesis (c.f., Stachel and Harris 2008). All other enstatites coexisting with clinopyroxene fall into the lherzolitic field (**Fig. 4b**). A magnesium-rich enstatite (Mg# 93.9) from a Frutal diamond, which cannot be assigned to a specific paragenesis based on co-existing inclusions, has CaO-Mg# characteristics that suggest a likely harzburgitic paragenesis (**Fig. 4b**).

Cr-diopside occurs in four diamonds, both as touching or non-touching associations with olivine, enstatite and Cr-pyrope (**Fig. 3a and b, *5*a and b**). The typical emerald-green color of Cr-diopside is not very saturated in the studied samples, with Cr_2O_3 contents varying from 0.47 to 1.18 wt%. Mg# varies from 93.8 to 94.5, except for the one augite grain (Mg# 88.9; sample DRP01) that forms a touching pair with the websteritic enstatite described above. Intergrowth/exsolution of orthopyroxene and clinopyroxene is a common feature in websteritic and transitional websteritic-lherzolitic diamonds from Voorspoed (Viljoen et al. 2018) and Namibia (Leost et al. 2003). Like the touching enstatite, the low Mg# of this clinopyroxene is comparable to transitional websteritic-lherzolitic clinopyroxenes from Voorspoed, but at lower CaO and higher TiO_2 contents. High Ca in enstatite and low Ca in clinopyroxene document a high formation temperature for this websteritic inclusion pair (Brey and Köhler 1990; see below). Relative to the lherzolitic Cr-diopsides from this study, the websteritic crystal has an elevated jadeite content and is Cr poor.

Purple **Cr-pyrope** was found in two diamonds from Douradinho River and one diamond from Abaeté (**Fig. 3a and d**). Based on chemical composition (**Fig. 4c**) and consistent with their coexistence with Cr-diopside, two garnets are assigned to the lherzolitic paragenesis. The third garnet, from Douradinho River, does not coexist with other minerals and despite a formal harzburgitic designation (classification of Grütter et al. 2004), falls right onto the compositional boundary between harzburgitic and lherzolitic garnets (**Fig. 4c**). In addition, this garnet has the lowest Mg# (85.1) of the set, which is closer to the average value for worldwide lherzolitic inclusions (84.7) than to harzburgitic inclusions (88.2; Stachel and Harris 2008), consistent with a lherzolitic origin. In general, Mg# from the studied garnets, varying from 85.1 to 86.5, are

253 relatively high compared to lherzolitic garnet inclusions worldwide (Stachel and Harris, 2008). Cr_2O_3 varies
254 widely between the analyzed crystals (5.44 to 12.8 wt%) and MnO content ranges from 0.23 to 0.28 wt%
255 and is positively correlated to Cr_2O_3.

256 Black **Mg-chromite** occurred in two diamonds, one from Verde River and one from Douradinho
257 River, and based on composition (Mg# 57.2-57.9 and Cr# of 82.8-89.7, respectively) was assigned to the
258 peridotitic suite. The Mg-chromite from Verde River has an unusually high and variable ZnO content (0.44
259 to 1.44 wt%) with an average value of 12 points (0.88 wt%) presented in **Supplementary Data 1**. High Zn
260 chromites were previously reported as inclusions in diamonds from the Canastra area, in Brazil (Tappert et
261 al. 2006). The high Zn inclusion has a cubo-octahedral morphology and no fractures connecting to the
262 diamond surface were observed, excluding an epigenetic origin (**Fig. 3e**). One additional Mg-chromite,
263 with Cr# of 68.2, was identified as a minute (5 μm) inclusion in an olivine from an Abaeté diamond. The
264 composition of this chromite is poorly constrained due to analytical overlap with the host olivine. The low
265 Mg# (91.9) of the host olivine suggests a lherzolitic paragenesis.

266 *4.2.2. Major element chemistry of eclogitic inclusions*

267 **Omphacite** was recognized in five diamonds, showing both green and blue colors. The observed
268 colors cannot be linked to variations in chemical composition. Omphacite is included without and with
269 eclogitic garnet, both as touching and non-touching pairs, and always outnumbers garnet inclusions in the
270 same diamond (**Fig. 3f**). In one diamond, omphacite coexists with garnet and coesite (DRR04). Omphacite
271 contains up to 6.45 wt% NaO and up to 11.7 wt% Al_2O_3, with a near 1:1 correlation between Na and Al (r^2
272 = 0.98). Aluminum slightly predominates over Na + K in apfu, indicating the additional presence of a small
273 Tschermaks component. The Mg-number range is 58.4 to 69.8 and K_2O varies from 0.05 to 0.50 wt%. In
274 two Douradinho River diamonds, omphacite exsolved a TiO_2 phase, identified as rutile via Raman
275 spectroscopy (**Supplementary Fig. 1b**). In two diamonds, one from Douradinho River and one from Verde
276 River, small patches and veins of a SiO_2 and Al_2O_3 rich material were observed in two otherwise notably
277 K_2O poor omphacites (**Fig. 5c**).

278 Orange colored **pyrope-almandine** was recovered from four diamonds, two from Douradinho
279 River and two from Verde River, all coexisting with clinopyroxene (**Fig. 3f**). The garnets have a low Cr_2O_3
280 content (max. 0.04 wt%), low Mg# (34.1 to 41.2), and variably high CaO concentrations (from 7.15 to 13.4
281 wt%; **Fig. 4c**). Although falling into the normal compositional ranges for eclogitic garnet inclusions
282 worldwide (Stachel and Harris 2008), the studied garnets are notably Ti-rich (TiO_2 up to 1.48 wt%). The
283 only garnet with TiO_2 <1 wt% is in direct contact with the above mentioned omphacite crystal with rutile
284 exsolutions (**Fig. 5d**); a second, non-touching garnet in the same diamond has a TiO_2 content of 1.46 wt%.

High TiO_2 (>1 wt%) garnet inclusions are common in eclogitic diamonds from Argyle (Jaques et al. 1989; Stachel et al. 2018a) and Voorspoed (Viljoen et al. 2018) and widespread among low-Cr majoritic garnet inclusions in diamonds from the Juína area, Brazil (Wilding 1990, Burnham et al. 2015), and the Monastery (Moore et al. 1991) and Premier kimberlites (Korolev et al. 2018), South Africa. In the garnets studied here, TiO_2 is negatively correlated with Al_2O_3 and positively correlated with CaO and Na_2O (0.23 to 0.40 wt%).

Coesite coexists with pyrope-almandine and omphacite in a diamond from Douradinho River. One of the coexisting clinopyroxenes in this diamond contains the silica-rich patches and veins described above. The coesite composition is essentially pure silica and the crystal structure was confirmed via Raman spectroscopy (**Supplementary Fig. 1c**).

A golden colored, cubo-octahedral **sulfide** was recovered from one diamond from Verde River. Based on a low Ni content (1.69 wt%), it was assigned to the eclogitic paragenesis. The sulfide grain has a homogeneous composition and no exsolutions were observed. Fe and S contents are 56.7 and 38.5 wt%, respectively, matching the composition of pyrrhotite. Concentrations of Cu range from 0.73 to 2.64 wt%, with the average value of nine points (1.55 wt%) presented in Sup. Table 1.

4.2.3. Trace elements

Clinopyroxene and garnet trace element compositions (**Supplementary Data 2**) were analyzed via LA-ICP-MS and the resulting rare earth element patterns (REE_N, N = CI-chondrite normalized; McDonough and Sun 1995) patterns are presented in **Figure 6**. Coexisting assemblages document that LREE are preferentially partitioned into clinopyroxene while garnet is the main host for MREE and HREE.

Peridotitic clinopyroxenes have REE_N patterns with negative slopes for the $LREE_N$-$MREE_N$ or, in one instance, flat $MREE_N$-$HREE_N$. MREE and HREE are generally strongly depleted relative to CI-chondrite (**Fig. 6a)**. A clinopyroxene that occurs touching with enstatite in a lherzolitic diamond from Abaeté (ABT03 in **Fig. 5a**) has an incomplete REE_N pattern due to the small laser spot size used but nevertheless documents superchondritic concentrations of Eu, Ho, Er and Lu, with a positive $MREE_N$-$HREE_N$ slope. The single websteritic clinopyroxene (DRP01) has a humped pattern, peaking at Nd (~ 10x chondritic abundance), followed by a gradual drop-off to Lu (**Fig. 6a**).

Lherzolitic garnets either have sinusoidal REE_N patterns peaking at Ce-Nd and showing a minimum at Dy (at Douradinho River) or are strongly LREE depleted with a positive slope from Tb_N to Lu_N (at Abaeté; **Fig. 6b**). All three garnets have approximately chondritic Lu concentrations and enrichment in LREE decreases with increasing Mg#.

Omphacite has humped REE_N patterns, peaking at Nd for most samples, followed by negative slopes for $MREE_N$-$HREE_N$ (**Fig. 6c**). An omphacite from Douradinho River (DRR04), coexisting with garnet and coesite, has lower $LREE_N$ abundances and a steeper positive slope within LREE, peaking at Sm-Eu (**Fig. 6c**). Omphacite VRM17 from Verde River is unusual with a steep drop-off from Nd to Sm, followed by a negative slope within $MREE_N$ and relatively flat $HREE_N$.

Eclogitic garnets have steep positive slopes within $LREE_N$, up to Sm_N, followed by fairly flat $MREE_N$-$HREE_N$ at ~30x chondritic abundance (**Fig. 6d**). The highest LREE, with a chondritic La abundance, occur in a garnet from Verde River (VRM17).

4.3. Geothermobarometry

Application of various geothermobarometers to the studied touching and non-touching inclusion assemblages results in estimates of the pressure and temperature conditions of last equilibration or of diamond formation, respectively. Data for multiple inclusions of the same type (either touching or non-touching) within the same diamond were averaged.

Diamond ABT04 from Abaeté contains a non-touching lherzolitic assemblage of garnet, clinopyroxene, orthopyroxene and olivine allowing an evaluation of multi-phase equilibrium and consequent assessment of the reliability of the applicable mineral exchange thermobarometers used for the remaining diamonds: coexisting garnet and clinopyroxene, coexisting orthopyroxene and clinopyroxene, and olivine only (cf., Nimis and Grütter 2010). Equilibrium between clinopyroxene and orthopyroxene is documented by very good agreement of the Ca-in-opx (1036 °C, Brey and Köhler 1990), enstatite-in-cpx (1048 °C, Nimis and Taylor 2000) and two pyroxene (1069 °C, Taylor 1998) thermometers, calculated for a fixed pressure of 50 kbar. Equilibrium between garnet and the two pyroxenes is indicated by very similar temperature estimates to the pyroxene-based results using the Mg-Fe exchange between garnet and clinopyroxene (1109 °C; Krogh 1988). On the other hand, the temperatures given by the Al-in-olivine (1216 °C, Bussweiler et al. 2017; 1231 °C, De Hoog et al. 2010) and Cr-in-olivine (1215 °C, De Hoog et al. 2010) thermometers, although in mutual agreement, are noticeably higher, differing by 146 to 195 °C from the enstatite-in-clinopyroxene based estimates.

For lherzolitic diamond ABT03, containing a touching enstatite-Cr-diopside pair plus non-touching olivine and enstatite, the same difference was noticed between the olivine-based and pyroxene-based thermometry results. For the non-touching enstatite, the Ca-in-opx thermometer (Brey and Köhler 1990) gives a temperature of 1037 °C, while the olivine thermometers (Bussweiler et al. 2017; De Hoog et al. 2010) give temperatures between 1206 and 1222 °C.

Diamond DRR08 contains a touching assemblage of olivine-clinopyroxene-orthopyroxene and non-touching garnet, olivine and clinopyroxene inclusions. Disagreement between pyroxene, pyroxene-garnet and garnet-olivine based thermometers indicates disequilibrium for both the minerals in the touching assemblage and among the non-touching inclusions. Observation of disequilibrium for a touching inclusion assemblage is unusual and likely relates to incomplete re-equilibration to changing thermal conditions (e.g., Stachel and Luth (2015).

After application of the compositional filters of Grütter (2009), the single clinopyroxene thermometer of Nimis and Taylor (2000) in combination with the updated calibration of the Cr-in-cpx geobarometer of Sudholz et al. (2021) was applied to the inclusions in the two well-equilibrated lherzolitic diamonds from Abaeté (ABT04 and ABT03). For the non-touching assemblage of ABT04 we obtain a temperature of 1038 °C and a pressure of 45 kbar, while cpx touching with opx in ABT03 yields 1089 °C and 50 kbar. Clinopyroxene touching with opx from the single websteritic diamond (DRP01 from Douradinho River) records a much higher temperature and pressure of ~1350 °C and 63 kbar.

For the samples containing only olivine, temperatures were calculated with the Cr-in-olivine (De Hoog et al. 2010) and Al-in-olivine (Bussweiler et al. 2017; De Hoog et al. 2010) thermometers, assuming a fixed pressure of 50 kbar. This results in temperatures between 1209 and 1260 °C for olivine-bearing Douradinho River diamonds and between 1040 and 1171 °C for Abaeté and Frutal samples. Based on the above comparison with pyroxene thermometry, these olivine-based temperature estimates may, however, be 100-200 °C too high. The Cr correction for the Al-in-olivine thermometer assigns all Cr present to the trivalent state (De Hoog et al. 2010). High Cr contents in some olivine inclusions in diamond have, however, been interpreted to result from the presence of divalent Cr and, consequently, De Hoog et al. (2010) provided a second formulation of their thermometer without Cr correction. Temperatures calculated with that version of Al-in-olivine thermometer differ by -34 to +15 °C and, on average, are 16 °C lower, compared to the Cr-corrected version, which is within the average expected difference of 20 °C for the two calibrations (De Hoog et al., 2010).

The chromite inclusion in diamond DRS06 yields a temperature of 1194 °C (Zn-in-spinel; Ryan et al. 1996). Given the extremely high Zn content in chromite from diamond VRM11, the thermometer was not applied to this inclusion as it would result in an unrealistic low temperature estimate.

For the eclogitic garnet and clinopyroxene pairs (n=3), temperatures range from 1238 to 1280 °C (Krogh 1988), calculated at a fixed pressure of 50 kbar. A touching pair of garnet and clinopyroxene in diamond DRP05 results in a ~100 °C lower temperature.

5. Discussion

5.1. Diamond substrate - a heterogeneous mantle

Here we discuss the compositionally heterogeneous lithospheric mantle beneath the southwestern margin of the São Francisco Craton and compare the diamond inclusion data from this study with diamond and xenocryst data from adjacent areas. In our dataset, peridotite appears to be the dominant diamond substrate, followed by eclogite. The additional presence of exotic websteritic diamond sources is indicated by a single sample. This compositional heterogeneity is well represented in diamonds from Douradinho River only, where all paragenesis were recorded (n=10; where 6 are peridotitic, 3 are eclogitic and 1 is websteritic).

5.1.1. Re-fertilized peridotitic mantle

Olivines trapped within diamonds are reliable indicators of the depletion level in cratonic lithosphere (Pearson and Wittig 2014). The high abundance of inclusions with lherzolitic affinity observed in the Abaeté and Douradinho River populations (**Table 1;** 70% of peridotitic diamonds) indicates that the mantle beneath the Coromandel/Abaeté areas is less depleted, or more re-fertilized, compared to neighboring areas within the confines of the Sao Francisco Craton, as revealed by other diamond studies (Kaminsky et al. 2001; Tappert et al. 2006) (**Fig. 1**). Kaminsky et al. (2001) analyzed diamonds from the Rio da Prata system, located more than 100 km to the northeast of Coromandel (between Presidente Olegário and João Pinheiro), recording an average olivine Mg# of 93.4 (n=28), consistent with strongly depleted (harzburgitic) sources. Tappert et al. (2006) studied diamond inclusions from the Canastra area, ~200 km south of Coromandel, again documenting the predominance of highly magnesian (depleted) olivines (n=4; Mg# of 93.8) over possible lherzolitic olivine (n=1; Mg# of 91.5). The limited data obtained for Frutal diamonds in this study (n=2; **Table 1**), ~250 km to the southwest of Coromandel (**Fig. 1**), also indicate strongly depleted (harzburgitic) mantle sources, consistent with the olivine inclusion data from the nearby Canastra area (Tappert et al. 2006).

An overall lower degree of depletion in the mantle beneath the Coromandel area is also evident from our garnet inclusions and previously published xenocrysts data from five kimberlites in the Coromandel area (**Fig. 4c**; n=532; Andrade 2012; Andrade and Chaves 2011; Carvalho et al. 2022; Coldebella et al. 2020), which show an almost complete absence of harzburgitic garnets, indicating that the sub-cratonic lithospheric mantle beneath Coromandel experienced only comparatively low degrees of partial melting, or was strongly re-fertilized. The shaded area in **Figure 4c** includes 7363 analyses of garnet xenocrysts from five additional kimberlites in Coromandel area by DeBeers (Pereira and Fuck 2005; Skinner 1996). These data are consistent with the moderately depleted character observed here for

inclusions in diamond. In keeping with the olivine compositions, garnet from the neighboring Rio da Prata and Canastra areas reveals a more depleted mantle compared to Coromandel and Abaeté. Garnet inclusions studied by Kaminsky et al. (2001; n=4) indicate a highly depleted mantle source for Rio da Prata system diamonds, with CaO contents varying from 0.91 to 4.61 wt%. Xenocryst data for kimberlites from the Canastra area (n=1482) (Andrade 2012; Costa 2008; Hill et al. 2015) are also consistent with a higher degree of depletion in the sub-cratonic lithospheric mantle for that area.

In this study no inclusions were recovered from diamonds from Romaria. Literature data for inclusions in Romaria diamonds (Meyer and Svisero 1975; Svisero 1978) indicate the presence of heterogeneous diamond source rocks, similar to the Coromandel lithospheric mantle. For four diamonds, the previous work documented a harzburgitic garnet-enstatite pair, an eclogitic sulfide, a lherzolitic clinopyroxene (Cr-diopside), and an olivine with Mg# 92. Xenocryst data for Romaria (n=72) (Coelho 2010) register an overall mildly depleted signature, similar to Coromandel.

Steep positive $HREE_N$ slopes observed for the lherzolitic garnet inclusions of Abaeté and Douradinho River indicate highly depleted precursors for both areas (**Fig. 6b;** Stachel et al. 2004). Sinusoidal/LREE-enriched trace element patterns indicate that the lithospheric mantle under these areas was affected by metasomatism, re-fertilizing the original depleted substrates. The $LREE_N$-$HREE_N$ patterns observed for lherzolitic garnet inclusions in this study strictly differs from the low degree of sinuosity common to worldwide lherzolitic inclusions (Stachel et al. 2004; **Fig. 6b**). Unlike worldwide occurrences, garnets from the dominant lherzolitic diamond population from the Victor kimberlite, Canada, show a strong degree of sinuosity (Stachel et al. 2018b; **Fig. 6b**). Regarding the type of metasomatism (melt versus fluid), the widely used Zr/Y indicator (Griffin and Ryan 1995; **Fig. 7a**) shows that worldwide lherzolitic garnet inclusions invariably follow a melt metasomatic trend, while Victor lherzolitic garnets fall along a fluid metasomatic trend. In our case, the metasomatic agent cannot be determined from the Zr/Y ratios in garnet, as concentrations are too low, reflecting a depleted signature **(Fig. 7a)**. Nevertheless, the dominant sinusoidal character of the garnet REE_N patterns is indicative of fluid-dominated or mild melt-driven metasomatic overprint (e.g., Stachel and Harris 2008).

The intensity of metasomatic overprint for the Abaeté and Douradinho River areas, however, is markedly different. The one lherzolitic garnet from the Abaeté area, which has subchondritic LREE, fairly unfractionated La_N/Eu_N and low $LREE_N/HREE_N$ (**Fig. 6b**), is the least metasomatized of all the garnets. Following modelling by Shu and Brey (2015), the REE_N pattern of garnet ABT04 could be explained through equilibration of pre-metasomatic garnet with only ~0.15% carbonatitic melt (relative to garnet). The high Ti/Eu of the Abaeté garnet (**Fig. 7b**), however, implies modification through a medium carrying significant Ti, such as protokimberlite or megacryst magma (Kargin et al. 2016). The Douradinho River

garnets, showing sinusoidal REE_N patterns with LREE from 1 (DRR08) to 10x (DRS04) chondrite abundances, would be consistent with equilibration with ~1 to 3% of metasomatic carbonatitic melt. Based on their elevated Zr/Hf and moderately low Ti/Eu (**Fig. 7b**)**,** the Douradinho River garnets suggest metasomatic equilibration with a medium that is transitional between carbonatite and kimberlite melts.

Similar to the garnets, clinopyroxenes from lherzolitic diamonds from Douradinho River show highly fractionated REE_N patterns, with La at ~10x chondritic abundances and subchondritic $HREE_N$ (**Fig. 6a**)**.** The two clinopyroxenes from Abaeté have much lower LREE–HREE ratios than the Douradinho River clinopyroxene, with La at chondritic (ABT03) to subchondritic (ABT04) abundance, consistent with the mild metasomatic overprint inferred for garnet ABT04. Clinopyroxenes ABT03 and ABT04 both have positive $HREE_N$ slopes. ABT03 carries super-chondritic $MREE_N$-$HREE_N$ and has the highest level of Ti enrichment observed in this study. As discussed above, the high Ti for cpx in ABT03 is inconsistent with carbonatite-driven metasomatism and points to interaction with a proto-kimberlite or megacryst magma-like melt.

5.1.2. Evidence for a recycled oceanic crust component

Eclogitic xenocrysts recovered in the Coromandel area are rare compared to the relatively high abundance of eclogitic inclusions in diamonds (~30%) in this study and their documented occurrence in the larger region (Rio da Prata system, Kaminsky et al. 2001; Abaeté area, Meyer and Svisero 1975; Romaria, Svisero 1978; Canastra, Tappert et al. 2006). A similar situation exists for the Argyle lamproite, where, although more than 90% of diamonds are derived from eclogitic sources, not a single eclogitic xenocryst has ever been documented (Luguet et al. 2009; Stachel et al. 2018a).

Eclogitic garnet and clinopyroxene inclusions studied here have a restricted compositional range in Mg# (34-41 for garnet and 58-70 for clinopyroxene). Based on the Ca# (26-37, with molar Ca=100Ca/(Ca+Mn+Fe+Mg)) and Mg# of non-touching garnet inclusions, the protoliths can be classified as high-Ca (Ca# > 20) and low-Mg (Mg# < 60) (Aulbach and Jacob, 2016). Using the proposed mineral modes of Aulbach and Jacob (2016; 55% garnet and 45% cpx), whole-rock compositions were reconstructed for eclogitic diamonds with analyzed garnet and clinopyroxene inclusions (DRR04, DRP05, VRM17; **Supplementary Data 1**). High FeO (12.9-15.5 wt%) and low MgO (6.3-8.5 wt%) contents result in low Mg# (45 to 52), reflecting an evolved character of the eclogitic protoliths. The calculated bulk rock major-element compositions, with Al_2O_3 varying from 15.2 to 16.5 wt% and CaO from 10.9 to 13.6 wt%, are broadly similar to that of MORB (Gale et al. 2013). Such evolved compositions, combined with elevated Na and Ti contents and the presence of coesite inclusions, point to derivation as oceanic crust through recycling (Jacob 2004). This interpretation of recycled oceanic crust as the source of eclogitic inclusions in

diamonds is consistent with the widespread occurrence of eclogitic diamonds along craton margins, as observed at Orapa, Jwaneng, Argyle and Voorspoed (Aulbach et al. 2017; Richardson et al. 2004; Stachel et al. 2018a; Viljoen et al. 2018), where younger material was accreted to the cratonic nuclei via subduction (Shirey et al. 2001).

The flat $MREE_N$-$HREE_N$ patterns observed in garnets (**Fig. 6d**) provide further evidence for a low-pressure origin like MORB (Jacob 2004). Due to strong partitioning of Eu^{2+} into plagioclase (McKenzie and O'Nions, 1991), the presence of positive Eu anomalies ($Eu_N/Eu^* > 1.05$; $Eu^* = (0.5*Gd_N + 0.5*Sm_N)$) is commonly used to identify plagioclase accumulation and consequently gabbroic protoliths (Aulbach and Jacob 2016; Jacob 2004). Among the analyzed eclogitic garnets (n=4), only one from Verde River shows a minor positive Eu anomaly (VRT04; $Eu_N/Eu^* = 1.10$), while the other three garnets have small negative anomalies ($Eu_N/Eu^* = 0.87$ to 0.93). Therefore, gabbros located in the deeper portions of oceanic crust are not the principle protolith for the eclogitic diamond substrates but instead basaltic pillow lavas and sheeted dikes from the shallow oceanic crust that experienced minor plagioclase fractionation dominate. Due to strong Sr partitioning into plagioclase (McKenzie and O'Nions, 1991), plagioclase fractionation should also be documented by negative Sr anomalies in photoliths. Calculated bulk trace element patterns (**Supplementary Data 2**) display negative Sr anomalies ($Sr_N/Sr^* < 1.05$; $Sr^* = (0.5*Pr_N + 0.5*Nd_N)$, with Sr_N/Sr^* varying from 0.8 to 1.02, consistent with the observation of minor negative Eu anomalies.

Bulk rock trace element patterns show a positive slope within the $LREE_N$ and almost flat $MREE_N$–$HREE_N$ at ~20x chondritic abundance (**Fig. 7c**). MREE-HREE for calculated Douradinho River bulk rocks perfectly matche NMORB (Gale et al. 2013) while the Verde River bulk rock falls slightly below NMORB. LREE are depleted relative to NMORB for all calculated bulk rocks (**Fig. 7c**). Such LREE depletion combined with NMORB-like MREE-HREE patterns indicates extraction of 10-20% melt in the garnet facies during protolith subduction (e.g., Stachel et al. 2004). A peak at Nd for one calculated bulk rock (VRM17) and a slightly concave slope in the $LREE_N$ for DRP05 suggest that melt depletion was followed by minor metasomatic re-enrichment in highly incompatible trace elements such as the LREE.

Low Mg# of the analyzed garnets, omphacites and calculated bulk rocks indicate that the eclogitic diamond substrates did not have a cumulate origin, even for the one sample with the slight positive Eu anomaly. Instead, major and trace element data suggest that the eclogitic diamond substrates originated from shallow subducted oceanic crust (pillow lavas and sheeted dikes), as already inferred from the presence of mild negative Eu anomalies in three samples.

5.1.3. Presence of a websteritic substrate

Websteritic suite diamonds are relatively rare, accounting for only ~2% worldwide (Stachel and Harris 2008). Their occurrence was first noted at Orapa (western edge of the Zimbabwe craton; Gurney et al. 1984), and other important localities with websteritic diamonds include Venetia (Limpopo Belt; Aulbach et al 2002), Voorspoed (eastern Witwatersrand Block of the Kaapvaal Craton; Viljoen et al. 2018), and the coastal deposits of Namibia (Leost et al 2003). Here, we report the first occurrence of a websteritic diamond in Brazil. The formation of websteritic diamond substrates has previously been related to reactions between slab-derived dacitic melts and peridotitic lithospheric mantle (Yaxley and Green 1998; Aulbach et al. 2002). Alternatively, an inclusion suite ranging from lherzolitic over lherzolitic-websteritic to websteritic in diamonds from the Voorspoed mine was interpreted to reflect plume impingement and melt infiltration of the lithospheric mantle during the 2.72 Ga Ventersdorp large igneous province (Viljoen et al. 2018).

The $MREE_N$-$HREE_N$ concentrations and pattern of the websteritic clinopyroxene from Douradinho River (DRP01) are similar to those of eclogitic clinopyroxenes (**Fig. 6c**). The positive slope within $LREE_N$, peaking at Nd-Sm, however, is steeper than observed for eclogitic omphacites. A minor negative Eu anomaly (Eu_N/Eu^*=0.96) observed for the websteritic clinopyroxene further suggests a link to subducted oceanic crust. Thus, for the case discussed here, the origin of the websteritic diamond substrate likely relates to hybridization of lithospheric lherzolite through reaction with eclogite-derived melt, as proposed in other studies (Aulbach et al., 2002; Smit et al. 2014; and references therein).

5.2. Pressure and Temperature Constraints

For the Abaeté area, a non-touching clinopyroxene (diamond ABT04) and a touching opx-cpx pair (ABT03), the former indicating the conditions of diamond formation and the latter the conditions of last equilibration, both follow a ~39 mW/m^2 model geotherm (Hasterok and Chapman 2011; **Fig. 8**). From Douradinho River, a touching pair of websteritic opx-cpx (DRP01) falls onto the high P-T end of the same conductive model geotherm. The calculated temperatures for the eclogitic diamonds from Douradinho and Verde rivers (average 1257 ± 23°C) indicate that they formed at unusually hot conditions, compared to worldwide eclogitic inclusions (mean: 1174 °C; Stachel and Harris 2008). Similar high temperatures are documented for eclogitic diamonds from Argyle (mean: 1250 °C; Stachel et al. 2018a). Further support for eclogitic diamond formation at high temperatures comes from the high Ti contents in the studied eclogitic garnet inclusions. The strong negative correlation between Ti and Al (r^2 = 0.97) observed for the eclogitic garnets indicates that Ti in garnet was mainly accommodated via substitution in the octahedral site. Aulbach (2020) argued that a temperature-dependent coupled substitution with Na is the dominant incorporation mechanism for Ti in garnet from mantle eclogite. Consequently, elevated Ti in the studied garnets indicates higher-than-average temperatures of diamond formation. The occurrence of rutile exsolutions then is a consequence of cooling after diamond formation, causing the solubility of Ti in garnet/clinopyroxene to

decrease. Further evidence for cooling after eclogitic diamond formation is provided by a ~100 °C lower temperature derived from touching (1184 °C) compared to non-touching (1280 °C) garnet-clinopyroxene in eclogitic diamond DRP05.

A paleo-geotherm for the study area was previously constructed by Read et al. (2004), using clinopyroxene xenocrysts from 95–89 Ma kimberlites in the Alto Paranaíba Igneous Province. Their data approximately correspond to a 37 mW/m^2 model geotherm (Hasterok and Chapman 2011). This geotherm falls below the ~39 mW/m^2 model geotherm derived here from touching and non-touching inclusions in diamond. Projecting the garnet-cpx thermometry for eclogitic inclusions onto a 39 mW/m^2 geotherm (**Fig. 8**) indicates a deep lithospheric origin. Projection onto a 37 mW/m^2 model geotherm results in even higher pressures, with some inclusions reaching temperatures in excess of the mantle adiabat. This observation, however, is not conclusive evidence against a conductive geotherm as low as the one derived by Read et al. (2004) and the observed difference of 2 mW/m^2 to our results is still considered within the uncertainty range of geothermobarometry-derived geotherms.

5.3. Time-averaged mantle residence temperatures based on nitrogen aggregation

The aggregation of nitrogen via diffusion in the diamond lattice is a time and temperature dependent process and mantle residence temperatures can be estimated using an approximation of mantle residence time and the interrelationship between nitrogen content and nitrogen aggregation state (**Fig. 9**; Taylor et al. 1990, 1996). In the absence of radiometric ages for diamonds from the Alto Paranaíba Province, we use indirect geological constraints to derive possible mantle residence times. The occurrence of eclogitic diamonds and the almost complete absence of peridotitic inclusions with a highly depleted, harzburgitic-dunitic character, point to diamond formation younger than 3.0 Ga (Shirey and Richardson 2011). In the context of the southwestern São Francisco Craton, subduction events with the potential to re-fertilize the lithospheric mantle and initiate growth of eclogitic and lherzolitic diamonds occurred during a Paleoproterozoic orogeny (2.2–1.9 Ga) and during the Brasiliano Orogeny (650–610 Ma) (Alkmim and Teixeira 2017; Barbosa and Barbosa 2017; Heilbron et al. 2017). The latter involved consumption of voluminous oceanic lithosphere of the Goiás-Pharusian Ocean, culminating in the formation of the Brasília Belt (Pimentel 2016). Kimberlites related to the Alto Paranaíba Igneous Province intruded in the Cretaceous (~90 Ma; Read et al. 2004).

Hence, we calculate “minimum” temperatures for diamond storage in the mantle considering a maximum residence time of 2.0 byr; shortening the residence time to 500 myr would increase mantle residence temperatures by only about 37 °C, on average. Two groupings in time-averaged equilibration temperatures can be identified (**Fig. 9**): 1) Residence temperatures >1200 °C, which include >90% of

Douradinho River samples, at least 50% of Abaeté samples, ~ 40% of Verde River samples and few samples from the Frutal and Romaria areas; 2) Residence temperatures <1150 °C, which includes most samples from the Frutal, Romaria and Verde River areas.

Average mantle residence temperatures (2.0 byr residence) are ~100 °C higher for Douradinho River samples (1270 °C) compared to the other studied diamond populations (Verde River: 1170 °C; Romaria: 1140 °C; Frutal: 1130 °C). No average residence temperature is given for Abaeté diamonds as only six samples were studied, of which two were Type IIa diamonds (no nitrogen detected). The high average residence temperature of Douradinho River samples matches that calculated for the eclogitic diamonds (1260 °C) and of the residence temperature of the single websteritic sample (1310 °C).

Compared to diamond populations worldwide, the residence temperatures for Douradinho River diamonds and, more specifically, for the eclogitic population from Douradinho and Verde rivers, are very high. Calculated for a shorter storage time of 0.5 byr, eclogitic diamonds from worldwide localities have an average mantle residence temperature of 1167 °C (Stachel et al. 2018a). Unusually high residence temperatures are, however, recognized for eclogitic diamonds from Argyle (average and median: 1300 °C; Stachel et al. 2018a). Recalculating the temperatures for eclogitic diamonds from the present study to 0.5 byr mantle residence (i.e., formation related to the Brasiliano Orogeny), then the average values increase from 1299 to 1342 °C. Temperatures for the eclogitic diamonds calculated at 2.0 byr mantle residence are, however, more consistent with the mineral inclusion geothermometry (**Table 1**), suggesting that a Paleoproterozoic orogeny is a more likely cause of diamond formation. The generally high temperatures for the eclogitic diamond population in the Coromandel area further show that the subducted oceanic crust likely accreted to the base of the lithosphere, similar to the case of the Argyle area (e.g., Jaques et al. 1989; Stachel et al. 2018a; Timmerman et al. 2019).

Peridotitic diamonds occur in both the low and high temperature groups. The very small number of diamonds with mineral inclusions in the low temperature group prevent a meaningful assessment of the involved diamond substrates. At Douradinho River diamonds, peridotitic (average: 1215 °C) and eclogitic (1295 °C) diamonds were both exposed to high time-averaged residence temperatures.

5.4. A diamond and mantle formation model for the Coromandel area

The nature of the cratonic lithosphere in the Coromandel area is poorly constrained due to Neoproterozoic (and younger) cover rocks occurring in the southwestern margin of the São Francisco Craton (Pimentel 2016) that obscure the basement and due to limited mantle xenolith studies. Based on diamond inclusion chemistry, we propose that the lithosphere underlying the Alto Paranaíba Igneous Province either is post-Archean, as previously suggested by Read et al. (2004), or represents originally

603 Archean lithosphere that was highly re-worked and re-enriched during Proterozoic times. **Figure 10**
604 illustrates our model for the formation of the different types of diamonds recognized in this study, as
605 discussed below.

606 The São Francisco Craton clearly comprises an Archean core (Teixeira et al. 2017). Dominantly
607 harzburgitic diamond populations typical of Archean depleted mantle were previously recognized at
608 Canastra and Rio da Prata areas (Kaminsky et al. 2001; Tappert et al. 2006). Our diamond inclusion study,
609 however, documents a less depleted, lherzolitic lithospheric mantle beneath the Alto Paranaíba region,
610 containing additional eclogitic and rare websteritic diamond sources. The eclogitic inclusion-bearing
611 diamonds from this study record low Mg# and reconstructed bulk rock trace element patterns consistent
612 with recycled oceanic crust. Two main orogenies could account for the subduction of oceanic crust in the
613 area: a Paleoproterozoic event (2.2-1.9 Ga) and the Brasiliano Orogeny (650-610 Ma) (Alkmim and
614 Teixeira 2017; Barbosa and Barbosa 2017; Heilbron et al. 2017). As mantle residence temperatures
615 calculated for 2.0 byr mantle residence are comparable to the formation temperatures of non-touching
616 eclogitic inclusions, an origin during a Paeloproterozoic orogeny is considered more likely. This
617 interpretation is supported by the presence of subduction-related segments of Paleoproterozoic orogens
618 occurring in the southernmost (Alkmim and Teixeira 2017) and northeastern portions (Barbosa and Barbosa
619 2017) of the São Francisco craton margin. The absence of strongly subcalcic garnets and an overall very
620 low proportion of harzburgitic garnets as xenocrysts in kimberlites characterizes lithosphere of late Archean
621 to Paleoproterozoic origin (c.f., Grütter et al. 1999; **Fig. 4c**). Lherzolitic diamonds are particularly abundant
622 in pericratonic/thermally-modified areas, as observed for the Victor mine (Superior Craton affected by 1.1
623 Ga Midcontinent rift; Stachel et al. 2018b), the Buffalo Hills kimberlites (Paleoproterozoic Buffalo Head
624 Terrane; Banas et al. 2007), and Ellendale olivine lamproites (Neoproterozoic King Leopold Orogen; Smit
625 et al. 2010). The dominantly lherzolitic and eclogitic diamond population recorded in the Alto Paranaíba
626 region is therefore consistent with post-Archean lithosphere. Re-depletion model ages of ~2.4 Ga derived
627 for peridotite xenoliths from mafic-alkaline rocks of the Alto Paranaíba Igneous Province (Carlson et al.
628 2007) provide further support for post-Archean lithosphere underlying the southwestern São Francisco
629 Craton.

630 Radiogenic isotope studies of magmatism in the region support the influence in the mantle of a
631 Paleoproterozoic orogeny. Kamafugitic, kimberlitic, and lamproitic rocks from the APIP have been studied
632 for Os-Sr-Nd-Pb isotope systematics, showing a lithospheric source for these magmas (Carlson et al. 1996).
633 In particular, the radiogenic Os of kamafugitic samples indicates pyroxenite/websterite/eclogite source
634 rocks in the lithospheric mantle, consistent with the eclogitic and websteritic diamond discovery in our
635 study for the same region. Pb isotope compositions of alkaline rocks in the southwestern part of the São

Francisco Craton indicate the influence of an old (>2 Ga) component in the lithosphere (Carlson et al. 1996). Similarly, a HIMU component (hybridization of an ancient subducted oceanic crust-derived melt with the ambient mantle; Hanyu et al. 2011) has been hypothesized to be present in the base of the lithosphere or brought up by a mantle plume (Bizzi 1996). The HIMU signature could also be created by a metasomatic overprint.

Projecting the hot temperatures of eclogitic diamonds onto a 39 mW/m² geotherm indicates formation between ~180 and 200 km depth. This is consistent, within error, with a seismically defined lithosphere/asthenosphere boundary at 181 km in the region (Priestley et al. 2018). The absence of a majorite component in the studied garnet inclusions, or of any other sublithospheric inclusions, suggests that sublithospheric diamond sources were not tapped during the Alto Paranaíba igneous event, unlike in the Juína region to the NW (Burnham et al. 2015; Wilding 1990).

5.4.1. Implications for diamond exploration

The results from this study motivate a reevaluation of best approaches to diamond exploration in the Alto Paranaíba region. The observed low abundance of diamonds with harzburgitic inclusions indicates that traditional exploration techniques, focusing on the presence of sub-calcic garnets in mineral concentrates (Gurney 1984), do not apply here. The prevalence of lherzolitic inclusions in diamonds from Alto Paranaíba (42%; comprising at least 67% of the peridotitic diamond population) highlights that exploration techniques must consider lherzolitic (G9) garnets as well. Although an effective way to explore for lherzolitic diamonds has not been developed to date, Grütter et al. (2004) showed that besides Cr_2O_3 in garnet as a barometric proxy, low MnO contents and Ca intercept values may indicate likely derivation of lherzolitic garnets from the diamond stability field. Another approach should consider the presence of lherzolitic xenocryst garnets displaying the same sinusoidal REE_N patterns frequently observed for lherzolitic inclusions. Sinusoidal REE_N patterns are not a common feature of lherzolitic garnet xenocrysts (Stachel et al. 2004), so if observed, the style of metasomatic overprint documented by such patterns may be employed to indicate the presence of lherzolitic substrates likely associated with diamonds.

Exploration for eclogitic diamond populations in the region (~30% of inclusion-bearing diamonds) is hampered by the low abundance of eclogitic garnets in the xenocryst record (**Fig. 4c**). This bias may imply limited preservation of eclogitic xenocrysts caused by the character of the magma(s) that brought the diamonds up to the Earth's surface (e.g., absence of eclogitic garnet xenocrysts in the Argyle lamproite; Stachel et al. 2018a). A recent study of an "exotic" kimberlite from the Coromandel area (Carvalho et al. 2022) reveals a rock with an enriched component in the magma source (including Ti-, Ca- and Zr-rich phases, atypical of kimberlites), sharing similarities with lamproites. Consequently, even a low abundance

of eclogitic garnets recovered during exploration may be a good indication for the likely presence of eclogitic diamonds.

6. Conclusions

Silicate inclusions in diamonds produced at Abaeté, Verde River and Douradinho River in the Alto Paranaíba Igneous Province, reveal a prevalence of the lherzolitic and eclogitic suites (>70%) and the first occurrence of a websteritic diamond in Brazil. This contrasts with findings for diamond populations from neighboring regions in the southwestern São Francisco Craton that formed dominantly in harzburgitic substrates. Consistently low levels of chemical depletion of peridotitic lithospheric mantle underlying the Alto Paranaíba Igneous Province, recorded in mineral inclusions from this study and in garnet xenocryst data compiled from literature, suggest either a post-Archean origin or significant re-enrichment and reprocessing of older mantle in the Proterozoic. Sinusoidal REE_N patterns of lherzolitic garnet inclusions are related to variably low levels of metasomatism by carbonatite-kimberlite or proto-kimberlite melts for the Coromandel and Abaeté areas in the Alto Paranaíba Igneous Province. Trace element patterns of eclogitic inclusions suggest derivation from upper sections of subducting slabs, while a single websteritic inclusion pair may relate to precipitation from eclogite-derived melts that were hybridized through interaction with ambient lherzolitic mantle. High temperatures calculated for the eclogitic and websteritic inclusion suites indicate crystallization near the base of the lithosphere. Very high aggregation states of nitrogen, observed especially in Douradinho River diamonds, indicate prolonged mantle residence at unusually high temperatures. Prolonged residence near the base of the lithosphere is consistent with the high abundance of deformed/brown diamonds and an origin related to Paleoproterozoic orogenic accretion and growth of the craton (2.2-1.9 Ga), rather than subduction and collision related to the relatively young Brasiliano Orogeny (0.65-0.61 Ga). The predominance of lherzolitic and eclogitic diamonds in the Alto Paranaíba region documented here, combined with the poor representation of eclogitic garnets among xenocryst populations, require new approaches to evaluate the diamond potential of kimberlite or kimberlite-like rocks carrying diamonds derived from these substrates.

Acknowledgments

The authors acknowledge the National Council for Scientific and Technological Development – CNPq (CNPq; 465613/2014-4) and the Foundation for Research Support of the Federal District (FAPDF; 193.001.263/2017) for financial support through INCT Estudos Tectônicos. L.D.V. Carvalho is grateful for

a PDSE scholarship sponsored by CAPES (88881.623483/2021-01) and a PhD scholarship granted by CNPq (169273/2017-2). T. Stachel and G. Pearson acknowledge funding through Natural Sciences and Engineering Research Council of Canada (NSERC) Discovery grants, which covered the analytical costs of this project. R. Fuck and R. Scholz acknowledge CNPq research fellowships. R. Scholz is grateful for FAPEMIG (PPM00588-18) and PROPP/UFOP (23109.000928/2020-33) grants. We thank A. Locock and Y. Luo for assistance with EPMA and ICPMS analyses. DIAMANDEL Mineração and GAR Diamond Mining are thanked for the donation of diamond samples. Mr. Osvaldo Soares França is thanked for valuable discussions about diamond occurrences in southwestern São Francisco Craton. Two anonymous reviewers are thanked for their constructive suggestions on the manuscript.

References

Alkmim, F.F., Teixeira, W., 2017. The Paleoproterozoic Mineiro Belt and the Quadrilátero Ferrífero. In: Heilbron, M., Cordani, U., Alkmim, F. (eds) São Francisco Craton, Eastern Brazil. Regional Geology Reviews. Springer, Cham. doi:10.1007/978-3-319-01715-0_5

Andrade, K.W., 2012. Química de minerais indicadores de intrusões kimberlíticas com ênfase na província diamantífera Serra da Canastra (MG): importância na prospecção de intrusões férteis. MSc. Dissertation UFMG. http://hdl.handle.net/1843/MPBB-8YYFRZ (in Portuguese)

Andrade. K.W., Chaves, M.L.S.C., 2011. Geologia e mineralogia do kimberlito Grota do Cedro (Coromandel, MG) Geonomos, 19 (1). doi:10.18285/geonomos.v19i1.61 (in Portuguese)

Aulbach, S., 2020. Temperature-dependent rutile solubility in garnet and clinopyroxene from mantle eclogite: Implications for continental crust formation and V-based oxybarometry. Journal of Petrology. doi:10.1093/petrology/egaa065

Aulbach, S., Jacob, D.E., 2016. Major- and trace-elements in cratonic mantle eclogites and pyroxenites reveal heterogeneous sources and metamorphic processing of low-pressure protoliths. Lithos, 262, 586–605. doi:10.1016/j.lithos.2016.07.026

Aulbach, S., Jacob, D.E., Cartigny, P., Stern, R.A., Simonetti, S.S., Wörner, G., Viljoen, K.S., 2017. Eclogite xenoliths from Orapa: Ocean crust recycling, mantle metasomatism and carbon cycling at the western Zimbabwe craton margin. Geochimica et Cosmochimica Acta, 213, 574–592. doi:10.1016/j.gca.2017.06.038

728 Aulbach, S., Stachel, T., Viljoen, S.K., Brey, G.P., Harris, J.W., 2002. Eclogitic and websteritic diamond
729 sources beneath the Limpopo Belt – is slab-melting the link? Contributions to Mineralogy and Petrology,
730 143(1), 56–70. doi:10.1007/s00410-001-0331-8

731 Banas, A., Stachel, T., Muehlenbachs, K., McCandless, T.E., 2007. Diamonds from the Buffalo Head Hills,
732 Alberta: Formation in a non-conventional setting. Lithos, 93(1-2), 199–213.
733 doi:10.1016/j.lithos.2006.07.001

734 Barbosa, J.S.F., Barbosa, R.G., 2017. The Paleoproterozoic Eastern Bahia Orogenic Domain. In: Heilbron,
735 M., Cordani, U., Alkmim, F. (eds) São Francisco Craton, Eastern Brazil. Regional Geology Reviews.
736 Springer, Cham. doi:10.1007/978-3-319-01715-0_4

737 Bardet, M.G., 1977. Geólogie du diamante. Troisième partie: Gisementes de diamants d'Asie, d'Amérique,
738 d'Europeet d'Australasie. Mémoires du Bur. Recherches Geol. Min., 83.169 p. (In French)

739 Bizzi, L.A., 1996. Mesozoic alkaline volcanism and mantle evolution of the southwestern São Francisco
740 craton, Brazil. PhD thesis. University of Cape Town.

741 Brey, G.P., Köhler, T., 1990. Geothermobarometry in Four-phase Lherzolites II. New Thermobarometers,
742 and Practical Assessment of Existing Thermobarometers. Journal of Petrology, 31(6), 1353–1378.
743 doi:10.1093/petrology/31.6.1353

744 Burnham, A.D., Thomson, A.R., Bulanova, G.P., Kohn, S.C., Smith, C.B., Walter, M.J., 2015. Stable
745 isotope evidence for crustal recycling as recorded by superdeep diamonds. Earth and Planetary Science
746 Letters, 432, 374–380. doi:10.1016/j.epsl.2015.10.023

747 Bussweiler, Y., Brey, G.P., Pearson, D.G., Stachel, T., Stern, R.A., Hardman, M.F., … Jackson, S.E., 2017.
748 The aluminum-in-olivine thermometer for mantle peridotites — Experimental versus empirical calibration
749 and potential applications. Lithos, 272-273, 301–314. doi:10.1016/j.lithos.2016.12.015

750 Bussweiler, Y., Giuliani, A., Greig, A., Kjarsgaard, B.A., Petts, D., Jackson, S.E., Barrett, N., Luo, Y.,
751 Pearson, D.G., 2019. Trace element analysis of high-Mg olivine by LA-ICP-MS – Characterization of
752 natural olivine standards for matrix-matched calibration and application to mantle peridotites. Chemical
753 Geology, 524, 136-157. doi:10.1016/j.chemgeo.2019.06.019

754 Carlson, R.W., Araujo, A.L.N., Junqueira-Brod, T.C., Gaspar, J.C., Brod, J.A., Petrinovic, I.A., Hollanda,
755 M.H.B.M., Pimentel, M.M., Sichel, S., 2007. Chemical and isotopic relationships between peridotite
756 xenoliths and mafic–ultrapotassic rocks from Southern Brazil. Chemical Geology.
757 doi:10.1016/j.chemgeo.2007.04.009

Carlson, R.W., Esperança, S., Svisero, D.P., 1996. Chemical and Os isotopic study of Cretaceous potassic rocks from Southern Brazil. Contributions to Mineralogy and Petrology, 125(4), 393–405. doi:10.1007/s004100050230

Carvalho, L.D.V., Jalowitzki, T., Scholz, R., Gonçalves, G.O., Rocha, M.P., Pereira, R.S., Lana, C., de Castro, M.P., Queiroga, G., Fuck, R.A., 2022. An exotic Cretaceous kimberlite linked to metasomatized lithospheric mantle beneath the southwestern margin of the São Francisco Craton, Brazil. Geoscience Frontiers, 13(1), 101281. doi:10.1016/j.gsf.2021.101281

Coelho, F.M., 2010. Aspectos geológicos e mineralógicos da mina de diamantes de Romaria, Minas Gerais. MSc dissertation. USP. https://doi.org/10.11606/D.44.2010.tde-24022011-113204 (in Portuguese).

Coldebella, B., Azzone, R.G., Chmyz, L; Ruberti, E., Svisero, D.P., 2020. Oxygen fugacity of Alto Paranaíba kimberlites and diamond instability: Três Ranchos IV and Limeira I intrusions. Brazilian Journal of Geology, 50 (1). doi:10.1590/2317-4889202020190087

Costa, G.V., 2008. Química mineral e geotermobarometria de xenólitos mantélicos do kimberlito Canastra-01. M.S. thesis, Universidade de Brasília, 137 p. (in Portuguese).

Day, H.W., 2012. A revised diamond-graphite transition curve. American Mineralogist, 97(1), 52–62. doi:10.2138/am.2011.3763

De Hoog, J.C.M., Gall, L., Cornell, D.H., 2010. Trace-element geochemistry of mantle olivine and application to mantle petrogenesis and geothermobarometry. Chemical Geology, 270(1-4), 196–215. doi:10.1016/j.chemgeo.2009.11.017

Evans, T., Kiflawi, I., Luyten, W., Vantendeloo, G., Woods, G.S., 1995. Conversion of platelets into dislocation loops and coidite formation in Type Iab diamonds: Proceedings of the Royal Society of London, Series A, Mathematical and Physical Sciences, v. 449, p. 295–313.

Gale, A., Dalton, C.A., Langmuir, C.H., Su, Y., Schilling, J.-G., 2013. The mean composition of ocean ridge basalts. Geochemistry, Geophysics, Geosystems, 14(3), 489–518. doi:10.1029/2012gc004334

Griffin, W.L., Ryan, C.G., 1995. Trace elements in indicator minerals: area selection and target evaluation in diamond exploration. Journal of Geochemical Exploration, 53(1-3), 311–337. doi:10.1016/0375-6742(94)00015-4

Grütter, H.S., 2009. Pyroxene xenocryst geotherms: Techniques and application. Lithos, 112, 1167–1178. doi:10.1016/j.lithos.2009.03.023

Grütter, H.S., Apter, D.B., Kong, J., 1999. Crust-mantle coupling: evidence from mantle-derived xenocrystic garnets. In: The JB Dawson Volume, Proceedings of the VIIth International Kimberlite Conference. Gurney JJ, Gurney JL, Pascoe MD, Richardson SH (eds) Red Roof Design, Cape Town, p 307–313

Grütter, H.S., Gurney, J.J., Menzies, A.H., Winter, F., 2004. An updated classification scheme for mantle-derived garnet, for use by diamond explorers☆. Lithos, 77(1-4), 841–857. doi:10.1016/j.lithos.2004.04.012

Gurney, J.J., 1984. A correlation between garnets and diamonds. In: Glover, J.E., Harris, P.G. (Eds.), Kimberlite occurrence and origins: a Basis for Conceptual Models in Exploration. Geology Department and University Extension, University of Western Australia, Publication 8 143– 166.

Gurney, J.J., Harris, J.W., Rickard, R.S., 1984. Silicate and Oxide Inclusions in Diamonds from the Orapa Mine, Botswana. Kimberlites - II: The mantle and crust - Mantle relationships, 3–9. doi:10.1016/b978-0-444-42274-3.50007-x

Hanyu, T., Tatsumi, Y., Senda, R., Miyazaki, T., Chang, Q., Hirahara, Y., Takahashi, T., Kawabata, H., Suzuki, K., Kimura, J-I., Nakai, S., 2011. Geochemical characteristics and origin of the HIMU reservoir: A possible mantle plume source in the lower mantle. Geochemistry, Geophysics, Geosystems, 12(2), 1–30. doi:10.1029/2010gc003252

Hasterok, D., Chapman, D.S., 2011. Heat production and geotherms for the continental lithosphere. Earth and Planetary Science Letters, 307(1-2), 59–70. doi:10.1016/j.epsl.2011.04.034

Heilbron, M., Cordani, U.G., Alkmim, F.F., 2017. The São Francisco Craton and Its Margins. In: Heilbron, M., Cordani, U., Alkmim, F. (eds) São Francisco Craton, Eastern Brazil. Regional Geology Reviews. Springer, Cham. doi:10.1007/978-3-319-01715-0_1

Hill, P.J.A., Kopylova, M., Russell, J.K., Cookenboo, H., 2015. Mineralogical controls on garnet composition in the cratonic mantle. Contributions to Mineralogy and Petrology, 169(2). doi:10.1007/s00410-014-1102-7

Jacob, D.E., 2004. Nature and origin of eclogite xenoliths from kimberlites. Lithos, 77(1-4), 295–316. doi:10.1016/j.lithos.2004.03.038

Jaques, A.L., Hall, A.E., Sheraton, J.W., Smith, C.B., Sun, S.-S., Drew, R.M., Foudoulis, C., Ellingsen, K., 1989. Composition of crystalline inclusions and C-isotopic composition of Argyle and Ellendale diamonds, in Ross, J. et al., eds., Kimberlites and related rocks. GSA Spec Publ 14, Volume 2: Carlton, Blackwell, p. 966-989.

817 Kaminsky, F.V., Zakharchenko, O.D., Khachatryan, G.K. Shiryaev, A.A., 2001. Diamonds from the
818 Coromandel area, Minas Gerais, Brazil. Revista Brasileira de Geociências, 31(4), pp.583-596.
819 doi:10.25249/0375-7536.2001314583596

820 Kargin, A.V., Sazonova, L.V., Nosova, A.A., Tretyachenko, V.V., 2016. Composition of garnet and
821 clinopyroxene in peridotite xenoliths from the Grib kimberlite pipe, Arkhangelsk diamond province,
822 Russia: Evidence for mantle metasomatism associated with kimberlite melts. Lithos, 262, 442–455.
823 doi:10.1016/j.lithos.2016.07.015

824 Korolev, N. M., Kopylova, M., Bussweiler, Y., Pearson, D. G., Gurney, J., Davidson, J., 2018. The uniquely
825 high-temperature character of Cullinan diamonds: A signature of the Bushveld mantle plume? Lithos, 304-
826 307, 362–373. doi:10.1016/j.lithos.2018.02.011

827 Krogh, E.J., 1988. The garnet-clinopyroxene Fe-Mg geothermometer – a reinterpretation of existing
828 experimental data. Contributions to Mineralogy and Petrology, 99(1), 44–48. doi:10.1007/bf00399364

829 Leost, I., Stachel, T., Brey, G.P., Harris, J.W., Ryabchikov, I.D., 2003. Diamond formation and source
830 carbonation: mineral associations in diamonds from Namibia. Contributions to Mineralogy and Petrology,
831 145(1), 15–24. doi:10.1007/s00410-003-0442-5

832 Luguet, A., Jaques, A.L., Pearson, D.G., Smith, C.B., Bulanova, G.P., Roffey, S.L., Rayner, M.J., Lorand,
833 J.-P., 2009. An integrated petrological, geochemical and Re–Os isotope study of peridotite xenoliths from
834 the Argyle lamproite, Western Australia and implications for cratonic diamond occurrences. Lithos, 112,
835 1096–1108. doi:10.1016/j.lithos.2009.05.022

836 McDonough, W.F., Sun, S.-s., 1995. The composition of the Earth. Chemical Geology, 120(3-4), 223–253.
837 doi:10.1016/0009-2541(94)00140-4

838 Mckenzie, D., O'Nions, R.K., 1991. Partial Melt Distributions from Inversion of Rare Earth Element
839 Concentrations. Journal of Petrology, 32(5), 1021–1091. doi:10.1093/petrology/32.5.1021

840 Meyer, H.O.A., Svisero, D.P., 1975. Mineral inclusions in Brazilian diamonds. Physics and Chemistry of
841 the Earth, v. 9, p. 785-795. doi:10.1016/0079-1946(75)90051-8

842 Moore, R.O., Gurney, J.J., Griffin, W.L. Shimizu, N., 1991. Ultra-high pressure garnet inclusions in
843 Monastery diamonds - trace element abundance patterns and conditions of origin. European Journal of
844 Mineralogy, 3(2): 213-230.

845 Nimis, P., Grütter, H., 2010. Internally consistent geothermometers for garnet peridotites and pyroxenites.
846 Contributions to Mineralogy and Petrology, 159(3), 411–427. doi:10.1007/s00410-009-0455-9

Nimis, P., Taylor, W.R., 2000. Single clinopyroxene thermobarometry for garnet peridotites. Part I. Calibration and testing of a Cr-in-Cpx barometer and an enstatite-in-Cpx thermometer. Contributions to Mineralogy and Petrology, 139(5), 541–554. doi:10.1007/s004100000156

Pearson, D.G., Wittig, N., 2014. The Formation and Evolution of Cratonic Mantle Lithosphere – Evidence from Mantle Xenoliths. Treatise on Geochemistry, 255–292. doi:10.1016/b978-0-08-095975-7.00205-9

Pereira, R.S., Fuck, R.A., 2005. Archean nucleii and the distribution of kimberlite and related rocks in the São Francisco craton, Brazil. Brazilian Journal of Geology, 35(3):93-104. doi:10.25249/0375-7536.200535S493104

Pereira, R.S., Fuck, R.A., França, O.S., Leite, A.A., 2017. Evidence of young, proximal and primary (YPP) diamond source occurring in alluviums in the Santo Antônio do Bonito, Santo Inácio and Douradinho rivers in Coromandel region, Minas Gerais. Brazilian Journal of Geology, 47(3), 383–401. doi:10.1590/2317-4889201720170047

Pimentel, M.M., 2016. The tectonic evolution of the Neoproterozoic Brasília Belt, central Brazil: a geochronological and isotopic approach. Brazilian Journal of Geology, 46(suppl 1), 67–82. doi:10.1590/2317-4889201620150004

Priestley, K., McKenzie, D., Ho, T., 2018. A Lithosphere-Asthenosphere Boundary-a Global Model Derived from Multimode Surface-Wave Tomography and Petrology. Geophysical Monograph Series, 111–123. doi:10.1002/9781119249740.ch6

Read, G., Grütter, H., Winter, S., Luckman, N., Gaunt, F., Thomsen, F., 2004. Stratigraphic relations, kimberlite emplacement and lithospheric thermal evolution, Quiricó Basin, Minas Gerais State, Brazil. Lithos, 77(1-4), 803–818. doi:10.1016/j.lithos.2004.04.011

Richardson, S.H., Shirey, S.B., Harris, J.W., 2004. Episodic diamond genesis at Jwaneng, Botswana, and implications for Kaapvaal craton evolution. Lithos, 77(1-4), 143–154. doi:10.1016/j.lithos.2004.04.027

Rocha, M.P., Azevedo, P.A.D., Assumpção, M., Pedrosa-Soares, A.C., Fuck, R., Von Huelsen, M.G., 2019. Delimiting the neoproterozoic São Francisco paleocontinental block with P-wave traveltime tomography. Geophysical Journal International, 219(1), 633-644. doi:10.1093/gji/ggz323

Ryan, C.G., Griffin, W.L., Pearson, N.J., 1996. Garnet geotherms: Pressure-temperature data from Cr-pyrope garnet xenocrysts in volcanic rocks. Journal of Geophysical Research: Solid Earth, 101(B3), 5611–5625. doi:10.1029/95jb03207

876 Shirey, S.B., Carlson, R.W., Richardson, S.H., Menzies, A., Gurney, J.J., Pearson, D.G., Harris, J.,
877 Wiechert, U., 2001. Archean emplacement of eclogitic components into the lithospheric mantle during
878 formation of the Kaapvaal Craton. Geophysical Research Letters, 28(13), 2509–2512.
879 doi:10.1029/2000gl012589

880 Shirey, S.B., Richardson, S.H., 2011. Start of the Wilson Cycle at 3 Ga Shown by Diamonds from
881 Subcontinental Mantle. Science, 333(6041), 434–436. doi:10.1126/science.1206275

882 Shu, Q., Brey, G.P., 2015. Ancient mantle metasomatism recorded in subcalcic garnet xenocrysts: Temporal
883 links between mantle metasomatism, diamond growth and crustal tectonomagmatism. Earth and Planetary
884 Science Letters, 418, 27–39. doi:10.1016/j.epsl.2015.02.038

885 Skinner, C., 1996. Prospecting in Western Minas Gerais, Brazil. Internal Report, De Beers Brasil, Brasília,
886 47p.

887 Smit, K.V., Shirey, S.B., Richardson, S.H., le Roex, A.P., Gurney, J.J., 2010. Re–Os isotopic composition
888 of peridotitic sulphide inclusions in diamonds from Ellendale, Australia: Age constraints on Kimberley
889 cratonic lithosphere. Geochimica et Cosmochimica Acta, 74(11), 3292–3306.
890 doi:10.1016/j.gca.2010.03.001

891 Smit, K.V., Stachel, T., Creaser, R.A., Ickert, R.B., DuFrane, S.A., Stern, R.A., Seller, M., 2014. Origin of
892 eclogite and pyroxenite xenoliths from the Victor kimberlite, Canada, and implications for Superior craton
893 formation. Geochimica et Cosmochimica Acta, 125, 308–337. doi:10.1016/j.gca.2013.10.019

894 Stachel, T., Aulbach, S., Brey, G.P., Harris, J.W., Leost, I., Tappert, R., Viljoen, K.S.Fanus., 2004. The
895 trace element composition of silicate inclusions in diamonds: a review. Lithos, 77(1-4), 1–19.
896 doi:10.1016/j.lithos.2004.03.027

897 Stachel, T., Banas, A., Aulbach, S., Smit, K.V., Wescott, P., Chinn, I.L., Kong, J., 2018b. The Victor Mine
898 (Superior Craton, Canada): Neoproterozoic lherzolitic diamonds from a thermally-modified cratonic root.
899 Mineralogy and Petrology. doi:10.1007/s00710-018-0574-y

900 Stachel, T., Harris, J.W., 2008. The origin of cratonic diamonds — Constraints from mineral inclusions.
901 Ore Geology Reviews, 34(1-2), 5–32. doi:10.1016/j.oregeorev.2007.05.002

902 Stachel, T., Harris, J.W., Hunt, L., Muehlenbachs, K., Kobussen, A.F., EIMF, 2018a. Argyle diamonds:
903 How subduction along the Kimberley Craton edge generated the world's biggest diamond deposit. In:
904 Geoscience and Exploration of the Argyle, Bunder, Diavik, and Murowa Diamond Deposits. Vol 20. Davy

AT, Smith CB, Helmstaedt H, Lynton Jaques A, Gurney JJ, (eds). Society of Economic Geologists, p 145–167. doi:10.5382/SP.20.06

Stachel, T., Luth, R.W. 2015. Diamond formation — Where, when and how? Lithos, 220-223, 200–220. doi:10.1016/j.lithos.2015.01.028

Sudholz, Z.J., Yaxley, G.M., Jaques, A.L, Brey, G.P., 2021. Experimental recalibration of the Cr-in-clinopyroxene geobarometer: improved precision and reliability above 4.5 GPa. Contributions to Mineralogy and Petrology 176, 11. doi:10.1007/s00410-020-01768-z

Svisero, D.P., 1978. Composição química, origem e significado geológico de inclusões minerais de diamantes do Brasil. Tese de Livre Docência. Universidade de São Paulo. 165 p. (in Portuguese)

Tappert, R., Stachel, T., Harris, J.W., Muehlenbachs, K. and Brey, G.F., 2006. Placer diamonds from Brazil: Indicators of the composition of the Earth's mantle and the distance to their kimberlitic sources. Economic Geology, 101(2): 453-470. doi:10.2113/gsecongeo.101.2.453

Taylor, W.R., 1998. An experimental test of some geothermometer and geobarometer formulations for upper mantle peridotites with application to the thermobarometry of fertile lherzolite and garnet websterite. Neues Jahrbuch Für Mineralogie - Abhandlungen, 172(2-3), 381–408. doi:10.1127/njma/172/1998/381

Taylor, W.R., Canil, D., Milledge, H.J., 1996. Kinetics of Ib to IaA nitrogen aggregation in diamond. Geochimica et Cosmochimica Acta, 60(23), 4725–4733. doi:10.1016/s0016-7037(96)00302-x

Taylor, W.R., Jaques, A.L., Ridd, M., 1990. Nitrogen-defect aggregation characteristics of some Australasian diamonds. Time-temperature constraints on the source regions of pipe and alluvial diamonds: American Mineralogist, v. 75, p. 1290–1310.

Teixeira, W., Oliveira, E.P., Marques, L.S., 2017. Nature and Evolution of the Archean Crust of the São Francisco Craton. In: Heilbron, M., Cordani, U., Alkmim, F. (eds) São Francisco Craton, Eastern Brazil. Regional Geology Reviews. Springer, Cham. doi:10.1007/978-3-319-01715-0_3

Timmerman, S., Honda, M., Zhang, X., Jaques, A.L., Bulanova, G., Smith, C.B., Burnham, A.D., 2019. Contrasting noble gas compositions of peridotitic and eclogitic monocrystalline diamonds from the Argyle lamproite, Western Australia. Lithos, 344-345, 193–206. doi:10.1016/j.lithos.2019.06.027

Viljoen, K.S., Perritt, S.H., Chinn, I.L., 2018. An unusual suite of eclogitic, websteritic and transitional websteritic-lherzolitic diamonds from the Voorspoed kimberlite in South Africa: Mineral inclusions and infrared characteristics. Lithos. doi:10.1016/j.lithos.2018.09.034

Wilding, M.C., 1990. A study of diamonds with syngenetic inclusions. PhD thesis, University of Edinburgh, Edinburgh, 281 pp.

Woods, G.S., 1986. Platelets and the infrared Absorption of Type Ia Diamonds. Proceedings of the Royal Society A: Mathematical, Physical and Engineering Sciences, 407(1832), 219–238. doi:10.1098/rspa.1986.0094

Yaxley, G.M., Green, D.H., 1998. Reactions between eclogite and peridotite: Mantle refertilisation by subduction of oceanic crust. Schweizerische Mineralogische und Petrographische Mitteilungen 78:243–255

Figure captions:

Figure 1: Simplified geological map showing the sampling locations of the diamond populations for this and previous studies in relation to the Neoproterozoic Brasília belt and the cover rocks of the Paraná (PRB) and São Francisco (SFB) basins. The indicated limit of the São Francisco paleocontinent is after Rocha et al. (2019). The boundaries of Minas Gerais (MG) with São Paulo (SP) and Goiás (GO) states are indicated.

Figure 2: Characteristics of the studied diamonds regarding a) color, b) morphology, c) nitrogen content and d) nitrogen aggregation state. In (b) the following abbreviations for morphologies are used: Oct/D-oct = Octahedral/dodecahedral-octahedral; Dod = Dodecahedral; Hemi = Pseudo-hemimorphic; Cleav = Cleavage fragment. In (d) diamonds are grouped according to the relative percentage of nitrogen in A and B centers (expressed as %A and %B), or the abundance of nitrogen (<5 ppm for Type IIa).

Figure 3: a) Garnet, clinopyroxene and olivine inclusions in diamond DRR08; on the right side, note a touching cpx-ol pair that is covered by a thick graphite layer. b) Released cpx-ol pair observed in (a) with thick graphite coating. c) Graphite coating of olivine inclusions and associated small fractures in a Douradinho river diamond. d) Olivine, greenish enstatite, and purple garnet in a lherzolitic diamond from Abaeté. e) Opaque chromite inclusion in a Verde River diamond. f) Eclogitic garnet and clinopyroxene in a diamond from Douradinho River; note a touching pair of grt-cpx and the bluish color of the non-touching cpx.

Figure 4: a) Cr_2O_3 vs. CaO contents (ppm) in olivines; the data points may be grouped according to their Mg#. The open circles correspond to samples assigned to the lherzolitic paragenesis based on coexistence with clinopyroxene. b) CaO vs. Mg# in enstatites from this study (see (a) for legend of symbols) and from websteritic and transitional websteritic-lherzolitic diamonds from Voorspoed

(Viljoen et al. 2018); the fields for the various parageneses are from Stachel and Harris (2008). c) Cr_2O_3 vs. CaO diagram for garnets with fields for parageneses after Grütter et al. (2004). Garnet inclusions from this study (large colored circles), garnet inclusions from previous studies (small colored diamonds; Kaminsky et al. 2001; Meyer and Svisero 1978; Tappert et al. 2006), and garnet xenocrysts from the Canastra (small triangles; Andrade 2012; Costa 2008; Hill et al. 2015), Romaria deposit (small squares; Coelho 2008), and Coromandel areas (small circles; Andrade 2012; Andrade and Chaves 2011; Carvalho et al. 2022; Coldebella et al. 2020; and shaded area representing the density of garnet xenocryst compositions from Skinner (1996) reported in Pereira and Fuck (2005)).

Figure 5: Backscattered electron images of a) touching pair of opx-cpx in a lherzolitic diamond from Abaeté; b) touching pair of opx-cpx in the single websteritic diamond from Douradinho River; c) cpx (light grey) containing a silica- and aluminum-rich phase (darker grey) in an eclogitic diamond from Douradinho River, and d) rutile exsolution in a grt-cpx touching pair from a Douradinho River diamond (photo of inclusion still inside diamond is shown as Fig. 3f).

Figure 6: CI-chondrite-normalized (McDonough and Sun 1995) REE element patterns of peridotitic (a) clinopyroxene and (b) garnet, and eclogitic (c) clinopyroxene and (d) garnet inclusions in diamonds. For comparison, the websteritic clinopyroxene DRP01 is presented in both (a) and (c) plots. Garnets and clinopyroxenes are represented by solid and dashed lines, respectively (see legend as inset in (d)). In (b), dotted lines represent calculated patterns for varying degrees of equilibration of garnet with 0.15 to 3% of a hypothetical carbonatitic melt (after Shu and Brey 2015). In grey, the field for lherzolitic inclusion garnets from Victor kimberlite is indicated (after Stachel et al. 2018b). Yellow shaded field indicates average composition of lherzolitic garnet inclusions from worldwide sources (after Stachel et al. 2004). For ABT03 and ABT04 clinopyroxenes, due to a very small laser beam (<33 µm), only a limited number of REE are above the limit of detection (as seen in (a)).

Figure 7: a) Y versus Zr plot (after Griffin and Ryan 1995) for lherzolitic garnet inclusions. Colored fields indicate the composition of lherzolitic garnet inclusions from worldwide localities (green) and the Victor kimberlite (blue) (after Stachel et al. 2018b); b) Zr/Hf versus Ti/Eu for lherzolitic garnet inclusions in diamonds. Indicated fields are after Shu and Brey (2015); c) CI-chondrite-normalized (McDonough and Sun 1995) REE for reconstructed eclogite bulk rock compositions from this study. The NMORB composition of Gale et al. (2013) is shown for reference.

Figure 8: Pressure and temperature conditions derived from clinopyroxene inclusions (Nimis and Taylor 2000; Sudholz et al. 2021) in two lherzolitic diamonds from Abaeté (filled and open orange circles) and the single websteritic diamond from Douradinho River (blue circle). Clinopyroxene

touching with orthopyroxene (diamond mantle residence conditions) is indicated as open symbols, isolated clinopyroxene (diamond formation conditions) as filled symbol. Temperatures for eclogitic garnet and clinopyroxene (open and filled symbols again for touching and non-touching inclusions, respectively; thermometer of Krogh 1988) in diamonds from Douradinho and Verde rivers, calculated for a fixed pressure of 50 kbar and (associated grey field with arrow) projected onto a 39mW/m² model geotherm. The diamond/graphite curve is from Day (2012). Geotherms and mantle adiabat are from Hasterok and Chapman (2011).

Figure 9: Nitrogen concentration vs. aggregation state (%B=$N_B/(N_A+N_B)$) for the different diamond sample populations studied (Abaeté = orange; Douradinho River = blue; Frutal = grey; Romaria = yellow; Verde River = green). The paragenesis of diamonds with analyzed mineral inclusions is indicated by the different symbol shapes. Isotherms are calculated after Taylor et al. (1990, 1996) for mantle residence times of 0.5 and 2 byr, as indicated.

Figure 10: Schematic model illustrating subcretion of a slab fragment beneath the southwestern margin of the São Francisco Craton during an accretionary event and the associated formation of the eclogitic, websteritic and lherzolitic diamonds observed in the present study. A minor harzburgitic diamond population present may predate this event. Eclogitic diamonds formed within the slab, either during subduction and associated prograde metamorphism or during subsequent fluid-driven diamond-forming events. The subduction and devolatilization of oceanic lithosphere caused refertilization of the overlying subcratonic lithospheric mantle, with consequent crystallization of lherzolitic diamonds. Slab-derived melts reacted with peridotite leading to precipitation of websteritic diamonds.

Table captions:

Table 1: Characteristic of the diamonds analyzed for their mineral inclusions. $T_{Nitrogen}$ for a mantle residence time of 2 byr calculated after Taylor et al. (1990, 1996). For diamonds with 0%B and with 100%B, the assumed detection limits for nitrogen B and A centers (1 and 99 %B) were used instead to obtain maximum and minimum residence temperature estimates, respectively.

Supplementary items

Figure captions:

Supplementary Figure 1: Representative Raman spectra of (a) graphite coat on olivine (diamond DRR08, shown as Fig. 3a), (b) rutile exsolutions (spectrum of non-touching omphacite from diamond DRP05), and (c) coesite inclusion in diamond DRR04. All spectra were recorded after inclusion extraction from the host diamond at room temperature.

Table caption:

Supplementary Table 1: Major element data (wt%) for mineral inclusions in diamond recovered in this study. For olivine, EPMA trace element analyses (ppm) for CaO, Al_2O_3 and Cr_2O_3 are provided as well. Bulk rock eclogite compositions were calculated based on 55% garnet and 45% clinopyroxene.

Supplementary Table 2: Trace element data for mineral inclusions, including calculated bulk rock trace element eclogite.

Figure 1

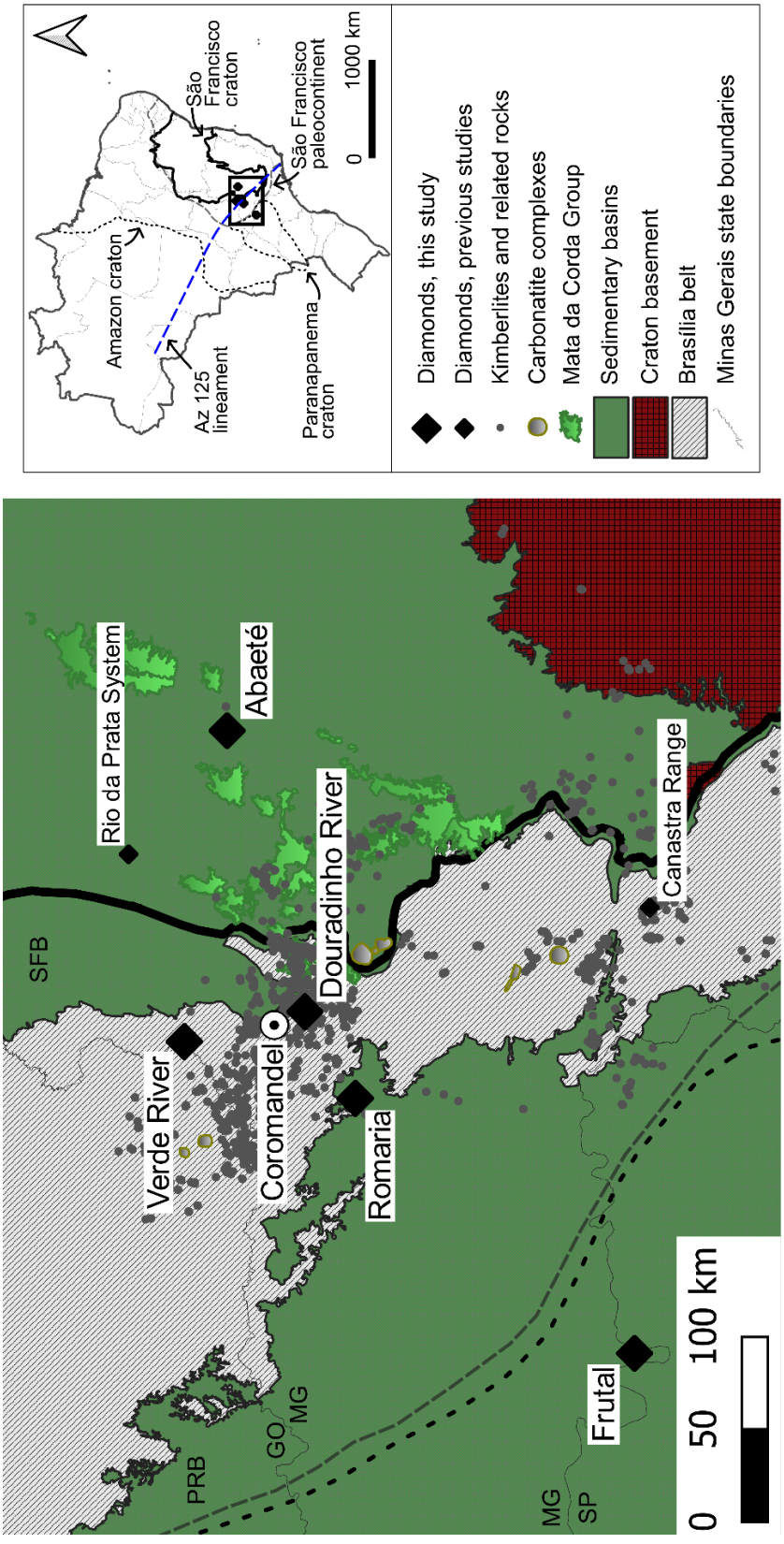
Rio da Prata System
Abaeté
Douradinho River
Canastra Range
SFB
Verde River
Coromandel
Romaria
PRB
GO
MG
Frutal
MG
SP
0 50 100 km
São Francisco craton
São Francisco paleocontinent
0 1000 km
Amazon craton
Az 125 lineament
Paranapanema craton
Diamonds, this study
Diamonds, previous studies
Kimberlites and related rocks
Carbonatite complexes
Mata da Corda Group
Sedimentary basins
Craton basement
Brasília belt
Minas Gerais state boundaries

Figure 2

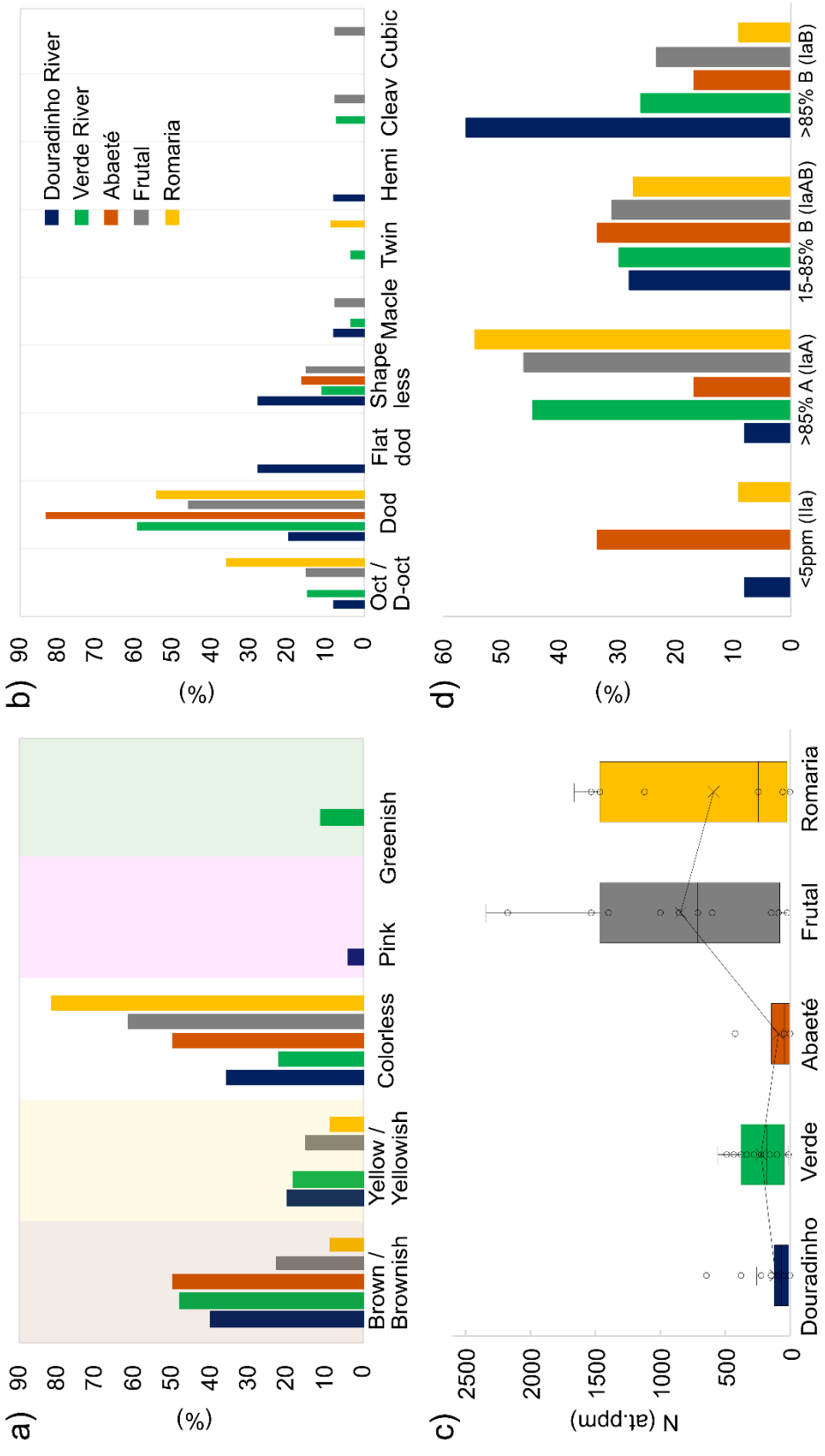
a)
(%)
Brown / Brownish
Yellow / Yellowish
Colorless
Pink
Greenish
b)
(%)
Douradinho River
Verde River
Abaeté
Frutal
Romaria
Oct / D-oct
Dod
Flat dod
Shape less
Macle
Twin
Hemi
Cleav
Cubic
c)
N (at.ppm)
Douradinho
Verde
Abaeté
Frutal
Romaria
d)
(%)
<5ppm (IIa)
>85% A (IaA)
15-85% B (IaAB)
>85% B (IaB)

Figure 3

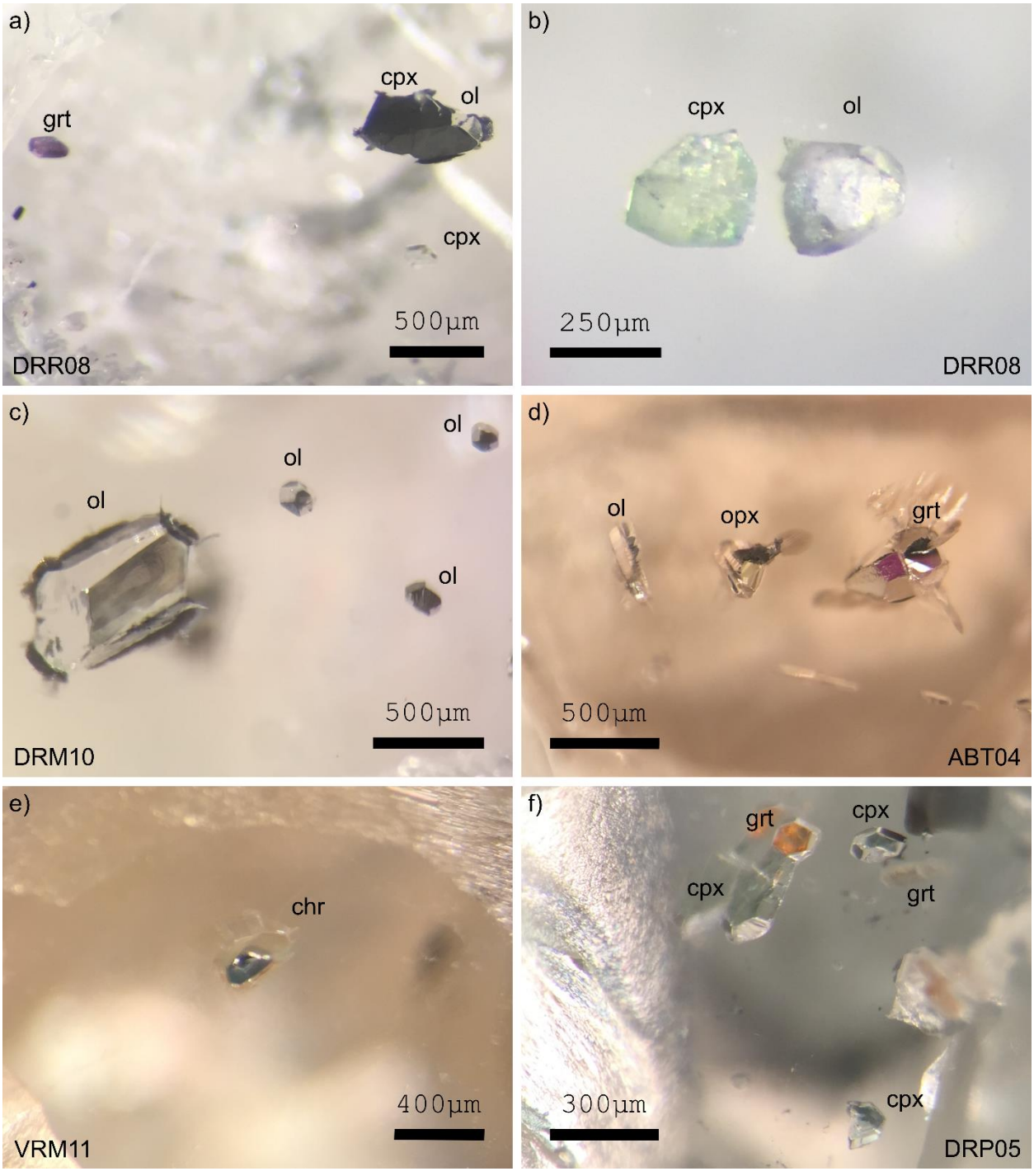
a)
grt
cpx
ol
cpx
500µm
DRR08
b)
cpx
ol
250µm
DRR08
c)
ol
ol
ol
ol
500µm
DRM10
d)
ol
opx
grt
500µm
ABT04
e)
chr
400µm
VRM11
f)
grt
cpx
cpx
grt
cpx
300µm
DRP05

Figure 4

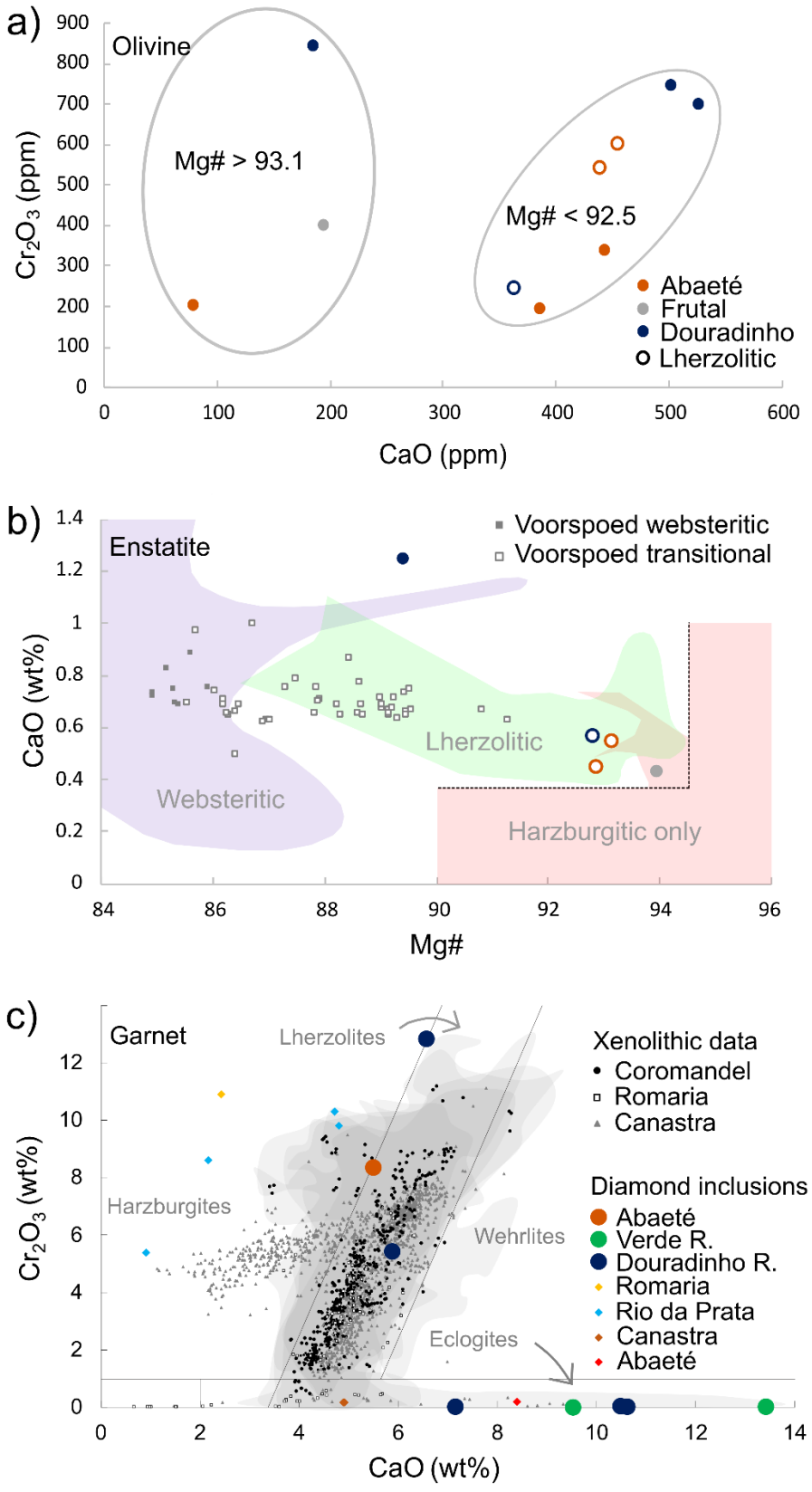
a)
Olivine
Mg# > 93.1
Mg# < 92.5
Abaeté
Frutal
Douradinho
Lherzolitic
Cr_2O_3 (ppm)
CaO (ppm)
b)
Enstatite
Voorspoed websteritic
Voorspoed transitional
Lherzolitic
Websteritic
Harzburgitic only
CaO (wt%)
Mg#
c)
Garnet
Lherzolites
Xenolithic data
Coromandel
Romaria
Canastra
Diamond inclusions
Abaeté
Verde R.
Douradinho R.
Romaria
Rio da Prata
Canastra
Abaeté
Harzburgites
Wehrlites
Eclogites
Cr_2O_3 (wt%)
CaO (wt%)

Figure 5

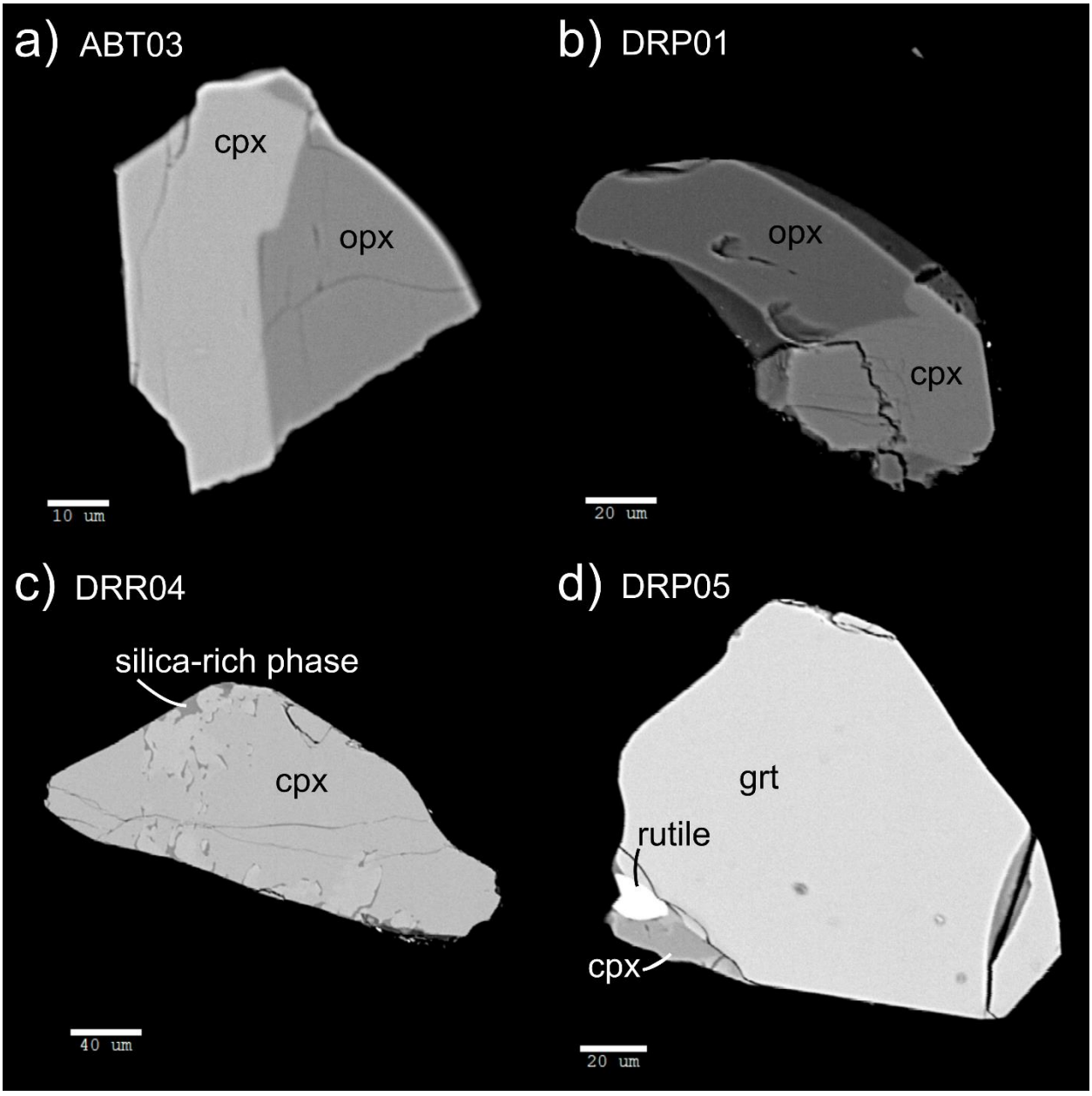
a) ABT03
cpx
opx
10 um
b) DRP01
opx
cpx
20 um
c) DRR04
silica-rich phase
cpx
40 um
d) DRP05
grt
rutile
cpx
20 um

Figure 6

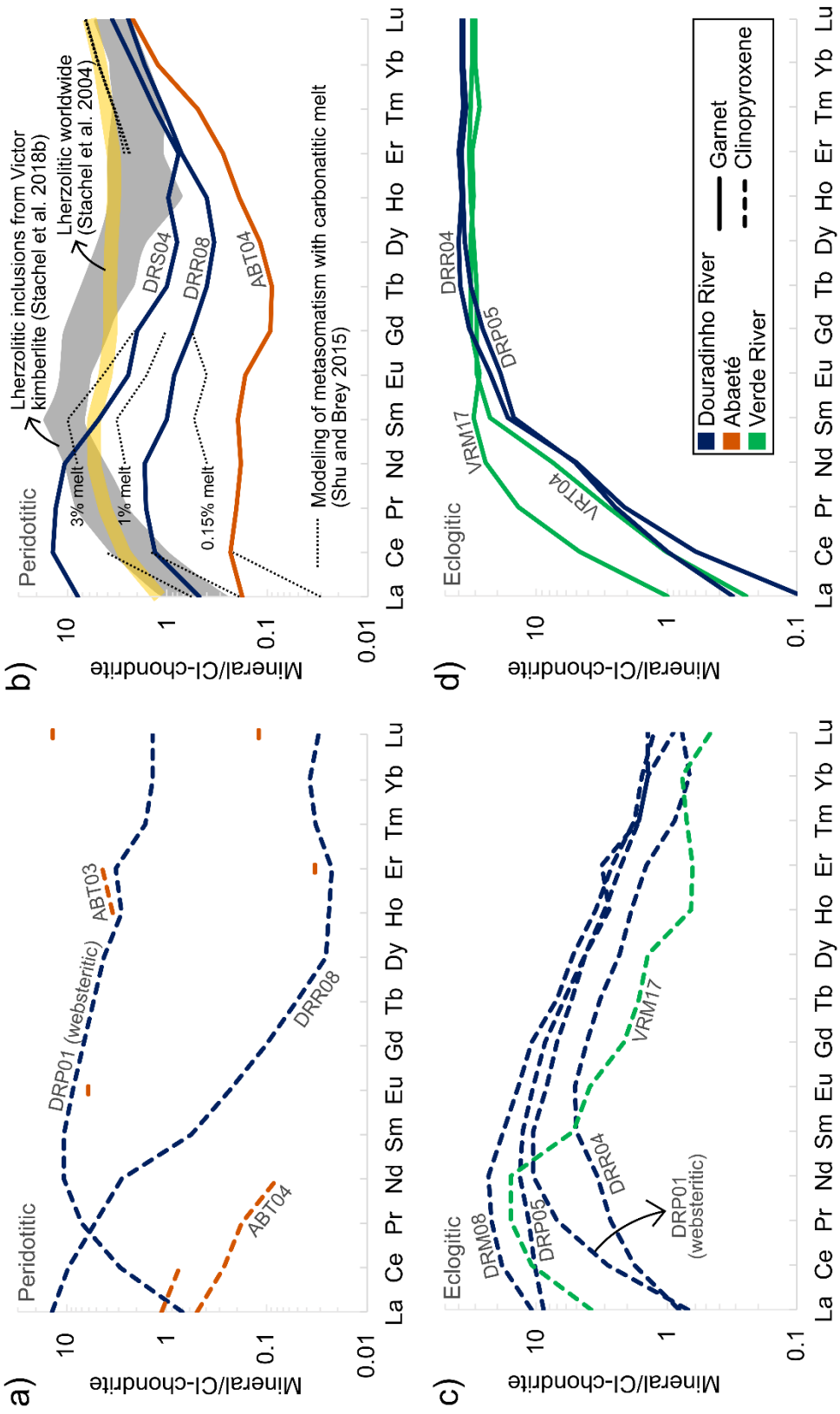
a)
Peridotitic
Mineral/Cl-chondrite
10
1
0.1
0.01
DRP01 (websteritic)
ABT03
ABT04
DRR08
La Ce Pr Nd Sm Eu Gd Tb Dy Ho Er Tm Yb Lu
b)
Peridotitic
Lherzolitic inclusions from Victor kimberlite (Stachel et al. 2018b)
Lherzolitic worldwide (Stachel et al. 2004)
3% melt
1% melt
0.15% melt
DRS04
DRR08
ABT04
Modeling of metasomatism with carbonatitic melt (Shu and Brey 2015)
c)
Eclogitic
DRM08
DRP05
DRR04
VRM17
DRP01 (websteritic)
d)
Eclogitic
DRR04
DRP05
VRM17
VRT04
Douradinho River
Abaeté
Verde River
Garnet
Clinopyroxene

Figure 7

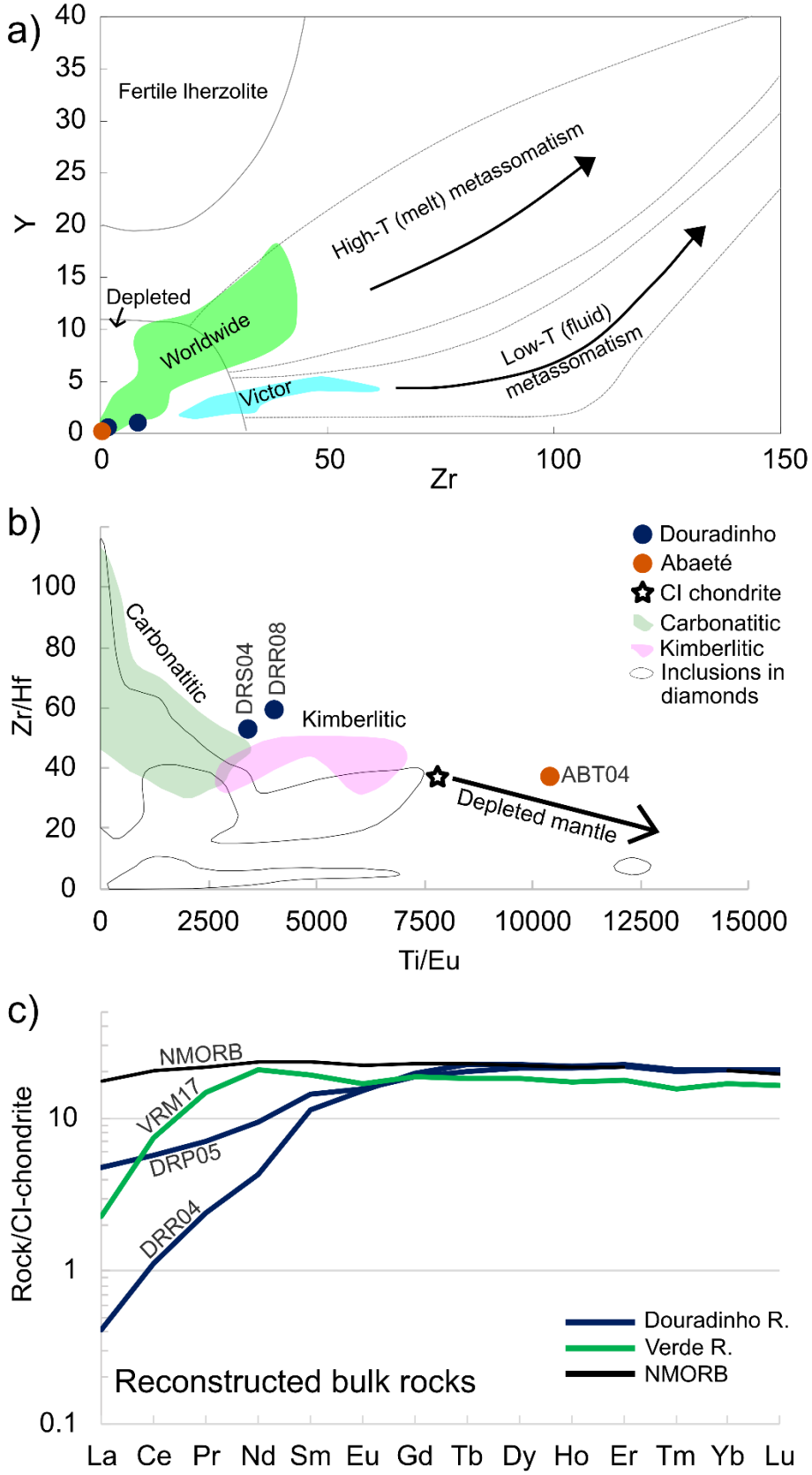
a)
Fertile lherzolite
High-T (melt) metassomatism
Depleted
Worldwide
Victor
Low-T (fluid) metassomatism
Y
Zr
b)
Douradinho
Abaeté
CI chondrite
Carbonatitic
Kimberlitic
Inclusions in diamonds
Carbonatitic
DRS04
DRR08
Kimberlitic
ABT04
Depleted mantle
Zr/Hf
Ti/Eu
c)
NMORB
VRM17
DRP05
DRR04
Douradinho R.
Verde R.
NMORB
Reconstructed bulk rocks
Rock/CI-chondrite
La Ce Pr Nd Sm Eu Gd Tb Dy Ho Er Tm Yb Lu

Figure 8

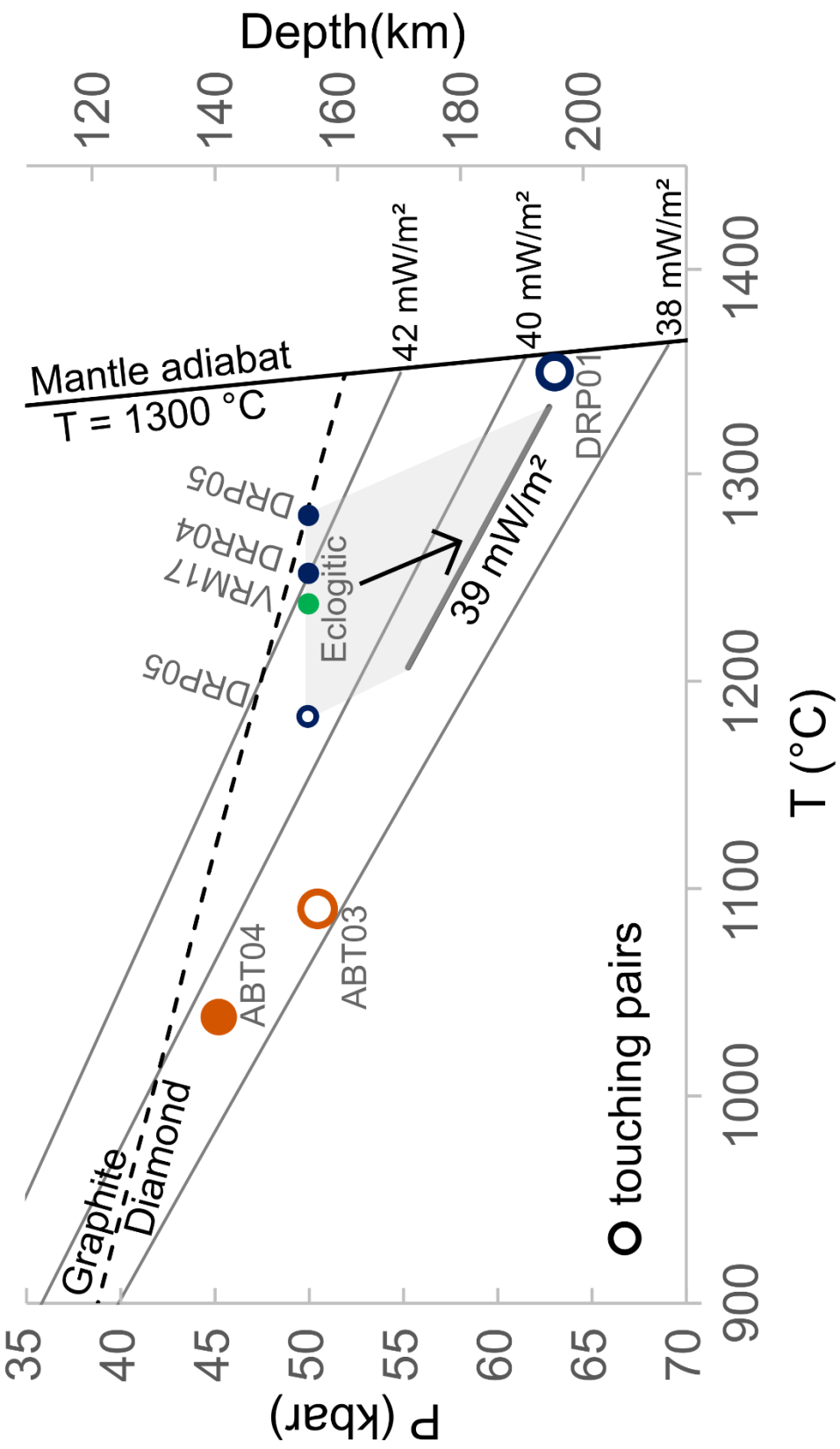
Depth(km)
120
140
160
180
200
42 mW/m²
40 mW/m²
38 mW/m²
Mantle adiabat
T = 1300 °C
DRP05
DRR04
VRM17
Eclogitic
39 mW/m²
DRP05
DRP01
ABT04
ABT03
Graphite
Diamond
touching pairs
35
40
45
50
55
60
65
70
P (kbar)
900
1000
1100
1200
1300
1400
T (°C)

Figure 9

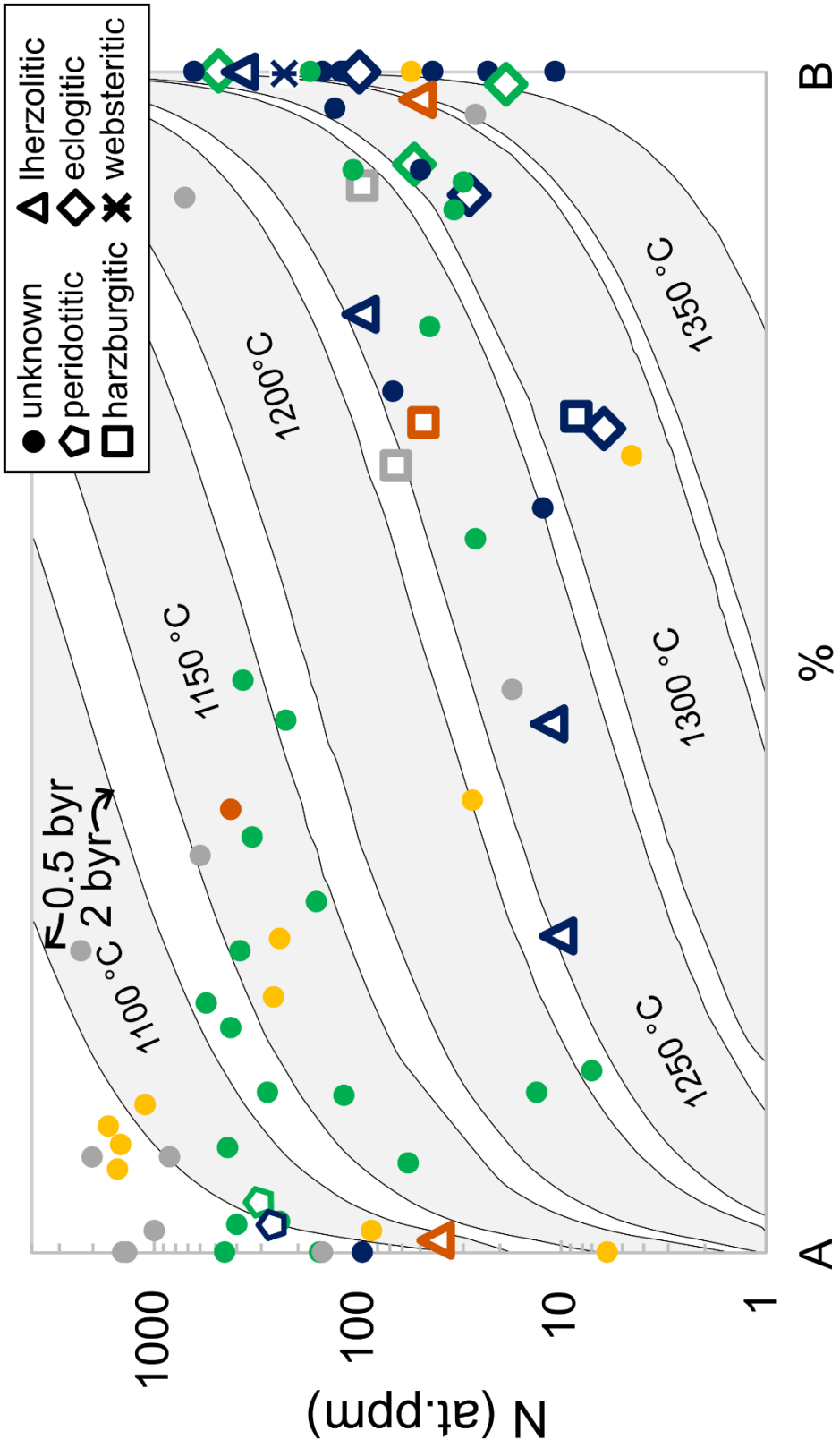
unknown
peridotitic
harzburgitic
lherzolitic
eclogitic
websteritic
0.5 byr
2 byr
1100 °C
1150 °C
1200 °C
1250 °C
1300 °C
1350 °C
N (at.ppm)
1000
100
10
1
A
B
%

Figure 10

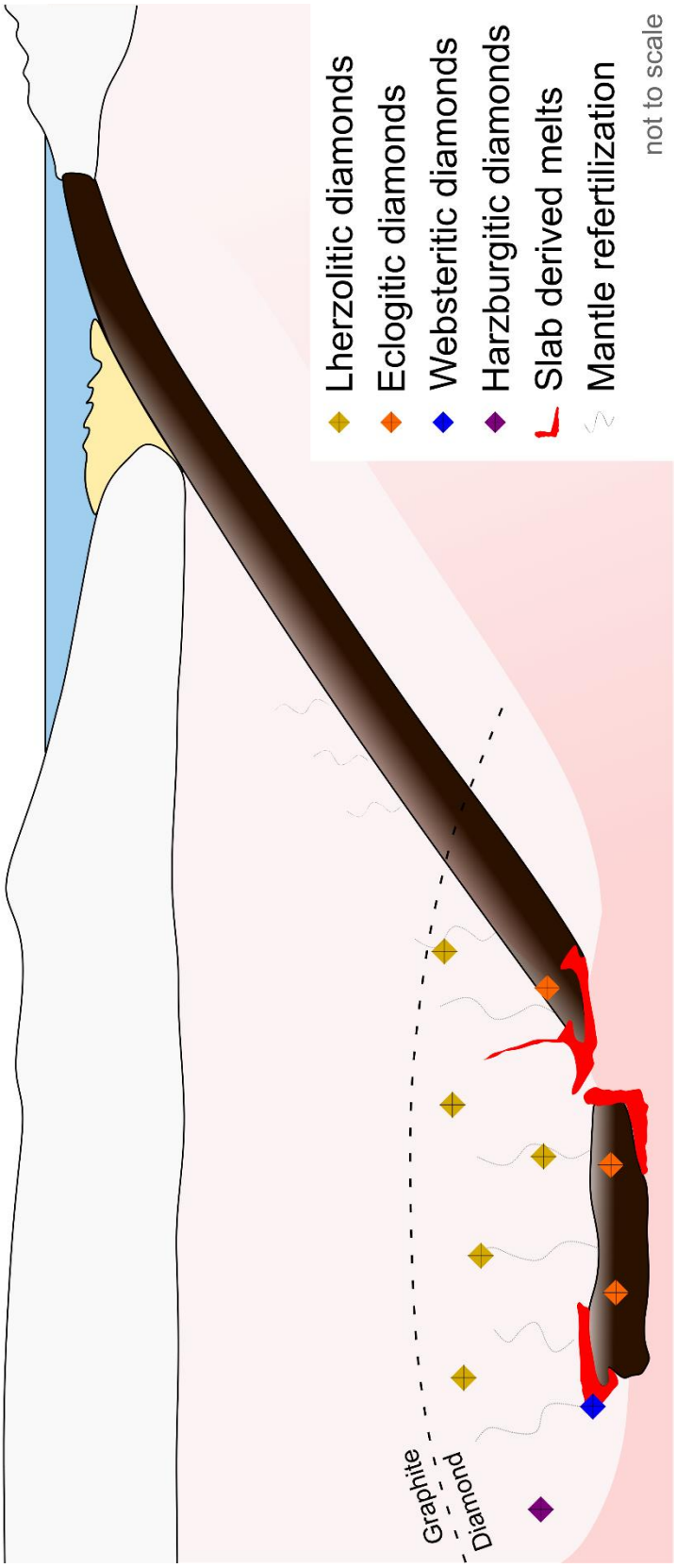
Lherzolitic diamonds
Eclogitic diamonds
Websteritic diamonds
Harzburgitic diamonds
Slab derived melts
Mantle refertilization
not to scale
Graphite
Diamond

Table 1

Diamond	Location	ct	Shape	Color	N at.ppm	%B centres	Mineral assemblage	Paragenesis	P-T estimates	TNitrogen***
ABT01	Abaeté	0.26	Shapeless	Colorless	42	0	Ol	Lherzolitic		1089
ABT02	Abaeté	0.28	Dodecahedron	Colorless	-	-	Ol	Lherzolitic		
ABT03	Abaeté	0.33	Dodecahedron	Brownish	-	-	Ol + Dio + En	Lherzolitic	50-1089*	
ABT04	Abaeté	0.37	Dodecahedron	Brownish	51	98	Ol + Dio + En + Grt	Lherzolitic	45-1038*	1303
ABT06	Abaeté	0.57	Dodecahedron	Colorless	46	70	Ol	Harzburgitic		1223
DRM01	Douradinho River	0.37	Octahedron	Yellowish	10	27	Ol	Lherzolitic		1213
DRM08	Douradinho River	1.12	Shapeless	Colorless	6	70	Omp	Eclogitic		1279
DRM10	Douradinho River	2.21	Flat dodecahedron	Colorless	8	71	Ol	Harzburgitic		1273
DRR01	Douradinho River	0.27	Hemimorphic	Colorless	12	45	Ol	Lherzolitic		1232
DRR04	Douradinho River	0.43	Dodecahedron	Yellow	29	89	Omp + Grt + Coe	Eclogitic	60-1294**	1273
DRR08	Douradinho River	1.73	Macle	Colorless	97	79	Ol + Dio + En + Grt	Lherzolitic		1216
DRS04	Douradinho River	0.21	Macle	Colorless	382	100	Grt	Lherzolitic		1290
DRS06	Douradinho River	0.30	Shapeless	Colorless	259	2	Chr	Peridotitic		1067
DRP01	Douradinho River	0.08	Shapeless	Colorless	226	100	Dio + En	Websteritic	63-1350**	1306
DRP05	Douradinho River	0.42	Shapeless	Colorless	100	100	Omp + Grt	Eclogitic	63-1332**	1331
FTB05	Frutal	0.27	Dodecahedron	Colorless	64	67	En	Harzburgitic		1210
FTM01	Frutal	0.04	Macle	Brownish	94	91	Ol	Harzburgitic		1243
VRM11	Verde River	0.20	Dodecahedron	Brownish	310	4	Chr	Peridotitic		1077
VRM15	Verde River	0.36	Dodecahedron	Colorless	495	100	Sulf	Eclogitic		1282
VRM17	Verde River	0.48	Dodecahedron	Yellowish	54	92	Omp + Grt	Eclogitic	59-1272**	1264
VRT04	Verde River	0.26	Dodecahedron	Colorless	19	99	Omp + Grt	Eclogitic		1361

Ol = olivine; Dio = diopside; En = enstatite; Grt = garnet; Omp = omphacite; Coe = coesite; Chr = chromite; Sulf = sulfide.

* Pressure (P) and temperature (T) iteratively calculated using Nimis and Taylor (2000) thermometer and Sudholz et al. (2021) barometer.

** P and T estimated by projecting the calculated temperatures of Krogh (1988) onto the 39 mW/m² geotherm of Hasterok and Chapman (2011).

*** Nitrogen-based temperature calculated for a mantle residence time of ~2.0 byr (after Taylor et al. 1990, 1996)

Supplementary Figure 1

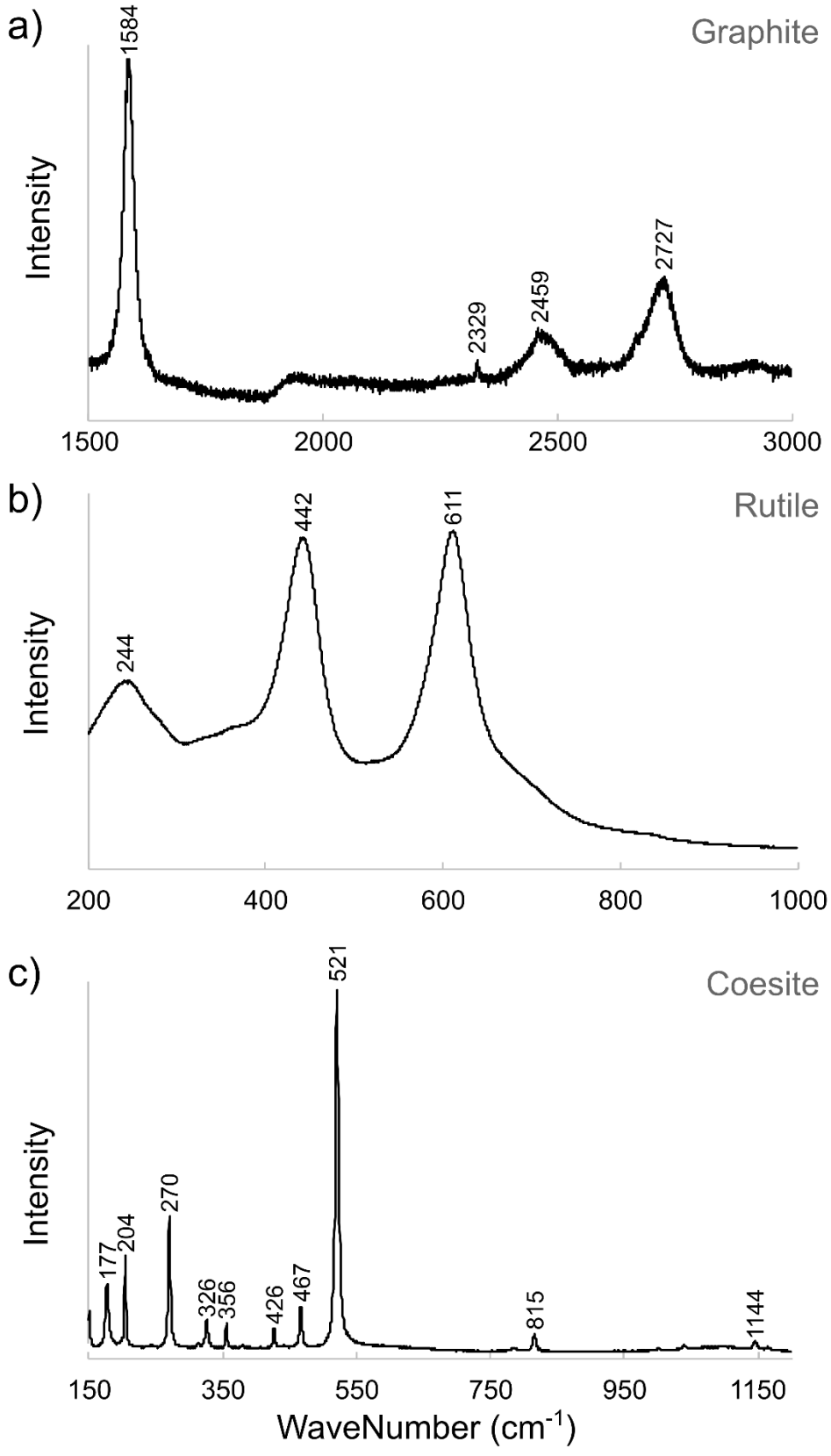

Supplementary Table 1

https://www.editorialmanager.com/lithos/download.aspx?id=1068965&guid=d59e8470-0669-4c73-b159-4e0626c89aa0&scheme=1

Supplementary Table 2

https://www.editorialmanager.com/lithos/download.aspx?id=1068966&guid=20ffd830-43d0-418f-a2dd-8f1195aaa41c&scheme=1